

18 **Abstract**

19 Northern peatlands in permafrost regions contain a large amount of organic carbon (C)
20 in the soil. Climate warming and associated permafrost degradation are expected to
21 have significant impacts on the C balance of these ecosystems, but the magnitude is
22 uncertain. We incorporated a permafrost model, Northern Ecosystem Soil
23 Temperature (NEST), into a biogeochemical model, DeNitrification-DeComposition
24 (DNDC), to model C dynamics in high-latitude peatland ecosystems. The enhanced
25 model was applied to assess effects of permafrost thaw on C fluxes of a sub-arctic
26 peatland at Stordalen, Sweden. DNDC simulated soil freeze/thaw dynamics, net
27 ecosystem exchange of CO₂ (NEE), and CH₄ fluxes across three typical land cover
28 types, which represent a gradient in the process of ongoing permafrost thaw at
29 Stordalen. Model results were compared with multi-year field measurements and the
30 validation indicates that DNDC was able to simulate observed differences in seasonal
31 soil thaw, NEE, and CH₄ fluxes across the three land cover types. Consistent with the
32 results from field studies, the modeled C fluxes across the permafrost thaw gradient
33 demonstrate that permafrost thaw and the associated changes in soil hydrology and
34 vegetation increase net uptake of C from the atmosphere, but also increase the annual
35 to decadal radiative forcing impacts on climate due to increased CH₄ emissions. This
36 study indicates the potential of utilizing biogeochemical models, such as DNDC, to
37 predict soil thermal regime in permafrost areas and to investigate impacts of
38 permafrost thaw on ecosystem C fluxes after incorporating a permafrost component
39 into the model framework.

40

41 **1 Introduction**

42 Northern peatlands are characterized by cold and wet conditions that promote the
43 accumulation of soil organic carbon (SOC) (e.g., Johansson T. et al., 2006; Schuur et
44 al., 2008). These ecosystems have accumulated 473-621 Pg (10^{15} g) carbon (C) since
45 the Last Glacial Maximum (Yu et al., 2010), with more than 277 Pg C stored in
46 permafrost areas (Schuur et al., 2008; Tarnocai et al., 2009). Although northern
47 peatlands generally acted as sinks of carbon dioxide (CO_2) in the past and under
48 current climate (e.g., Lund et al., 2010; McGuire et al., 2009); peat C stocks may be
49 released to the atmosphere with climate warming, due to mobilization of previously
50 frozen C in permafrost soils and accelerated decomposition of SOC (e.g., Frolking et
51 al., 2011; McGuire et al., 2009; Schuur et al., 2009, 2011). In addition, because of
52 prevailing anaerobic soil conditions, northern peatlands are an important source of
53 atmospheric methane (CH_4), releasing 31-65 Tg $\text{CH}_4 \text{ yr}^{-1}$ (McGuire et al., 2009) and
54 methane emissions can change with permafrost thaw (Christensen et al., 2004).

55

56 Pronounced warming has been observed in northern high latitudes, with surface air
57 temperature increased by approximately $0.09^\circ\text{C decade}^{-1}$ during the 20th century
58 (ACIA, 2005). More pronounced warming has been projected in this region for the
59 21st century (IPCC, 2007). Many recent studies have argued that the rate or extent of
60 permafrost degradation is increasing with climate warming in northern peatlands (e.g.,
61 James et al., 2013; Payette et al., 2004; Quinton et al., 2011; Åkerman and Johansson,
62 2008). Permafrost thaw can result in increases in active layer thickness (ALT; the
63 thickness of surface soil layer that freezes and thaws seasonally above a year-round
64 frozen layer) and cause land surface subsidence, which in turn may cause changes in
65 topography, soil hydrology, and vegetation (e.g., Avis et al., 2011; Johansson M. et al.,

66 2006; Schuur et al., 2008). These changes associated with permafrost degradation can
67 significantly affect the C cycle in northern ecosystems (e.g., Dorrepaal et al., 2009;
68 Johansson T. et al., 2006; McGuire et al., 2009; Schneider von Diemling et al., 2012).

69

70 Although much concern has been placed on the C balance in permafrost ecosystems,
71 large uncertainty still exists (e.g., Koven et al., 2011; McGuire et al., 2009; Schuur et
72 al., 2011). Northern peatlands are highly heterogeneous, usually with varying
73 characteristics of permafrost, topography, hydrology, soil, and vegetation within close
74 proximity (Nungesser, 2003), which results in considerable variations of C fluxes at
75 local and landscape scales (e.g., Bäckstrand et al., 2010; Lund et al., 2010; Sachs et
76 al., 2010). Responses of the C balance to permafrost degradation have been shown to
77 vary across different peatlands as well (Bäckstrand et al., 2010). Therefore, it is an
78 ongoing challenge to extrapolate site-specific measurements to large regions.

79

80 Process-based models are effective tools to assess the impacts of climate change on
81 boreal ecosystems. Several large-scale models have been enhanced by incorporating
82 thermal, hydrologic, vegetation, and biogeochemical processes in relation to
83 permafrost conditions and these models have been applied to quantify the impacts of
84 climate change on C fluxes at regional and global scales (e.g., Schneider von
85 Diemling et al., 2012; Wania et al., 2009a, 2009b; Zhuang et al., 2001, 2004, 2006).

86 Predictions by large-scale models are generally done at coarse spatial resolutions,
87 therefore may be deficient in considering the effects of local spatial heterogeneity. By
88 improperly considering fine-scale spatial heterogeneity in vegetation and
89 environmental conditions, systematic biases may occur in simulations of permafrost
90 degradation and C fluxes (Bohn and Lettenmaier, 2010; Zhang et al., 2013). In

91 addition, the results based on coarse-scale modeling are difficult to validate by
92 comparing with field observations and uncertainty may arise in regional and global
93 simulations due to limited validation (Kirschke et al., 2013).

94

95 A process-based biogeochemical model, DeNitrification-DeComposition (DNDC),
96 was recently enhanced by incorporating a permafrost model, Northern Ecosystem
97 Soil Temperature (NEST), for predicting biogeochemistry in high latitudes from plant
98 communities to ecosystem scale. The model was initially tested against one growing
99 season of CH₄ flux data measured at a permafrost site in the Lena River Delta, Russia
100 (Zhang et al., 2012). In this study, we applied the enhanced model to assess effects of
101 permafrost thaw on C fluxes of a well-studied sub-arctic peatland at Stordalen,
102 Sweden. The study peatland is located in a discontinuous permafrost zone and
103 consists of palsas – small, relatively dry plateaus elevated one to a few meters due to
104 subsurface ice lenses (Williams and Smith, 1989) – and intervening low, wetter areas.
105 These palsas can expand and shrink in extent with relatively small variations in
106 environmental conditions such as temperatures or winter snow packs (Payette et al.
107 2004), and represent one class of permafrost (Davis, 2001). Stordalen’s palsas are
108 extremely vulnerable to changing climate and widespread degradation of permafrost
109 is expected to occur (Åkerman and Johansson, 2008). DNDC simulated multi-year
110 soil freeze/thaw dynamics, net ecosystem exchange of CO₂ (NEE), and CH₄ fluxes
111 across three typical land cover types, which represent a gradient of permafrost
112 degradation in the study region. During simulations, different soil hydrologic
113 conditions and vegetation characteristics of these land cover types were used as
114 model inputs, therefore we focused on predicting the changes in soil thermal
115 dynamics and C cycling along with thawing. The model was tested against long-term

116 field measurements to verify its applicability for simulating the differences in soil
117 thermal regime and C fluxes across a gradient of permafrost thaw. Then we assessed
118 the possible impacts of permafrost thaw on C fluxes for the Stordalen peatland based
119 on the multi-year simulations. A validated simulation model provides a mechanism
120 for not only interpreting observations but also predicting the impacts of future climate
121 change on greenhouse gas emissions.

122

123 **2 Methods and data**

124 **2.1 The study area and field observations**

125 The study area is the Stordalen mire (68°20'N, 19°03'E, 351 ma.s.l.) located 10 km
126 southeast of Abisko Scientific Research Station (ANS) in northern Sweden. It is a
127 sub-arctic peatland with discontinuous permafrost. Peat formation at the mire
128 occurred at about 5000 cal. BP (Rosswall et al., 1975; Kokfelt et al., 2010). This area
129 has a continental climate, with an annual mean air temperature of 0.07 °C and an
130 average annual precipitation of 308 mm during 1986-2006 according to the
131 observations at ANS (Callaghan et al., 2010). Long-term climate records at ANS
132 indicate that the annual mean air temperature in this region has increased by 2.5 °C
133 from 1913 to 2006, significantly exceeding the 0 °C threshold for the first time during
134 the last few decades (Bäckstrand et al., 2008; Callaghan et al., 2010). This warming
135 has led to a thicker active layer and permafrost disappearance in this area (Åkerman
136 and Johansson, 2008). The degradation of permafrost has significantly affected
137 surface topography, hydrology, and vegetation, and thereby exerted a strong influence
138 on the fluxes of CO₂ and CH₄ (Christensen et al., 2004; Johansson T. et al., 2006;
139 Malmer et al., 2005; Åkerman and Johansson, 2008).

140

141 As in most peatlands in permafrost regions, Stordalen mire has high spatial
142 heterogeneity in topography (1-2 m relative differences in elevation). The topographic
143 variability creates small-scale (meters) environments with different soil moisture and
144 nutrient conditions that support different plant communities (Rosswall et al., 1975;
145 Bäckstrand et al., 2008). The area can be broadly classified into three typical land
146 cover types (i.e., dry Palsa, semi-wet Sphagnum, and wet Eriophorum; note that in
147 this study the terms Sphagnum and Eriophorum indicate land cover types instead of
148 vegetation species). The Palsa sites of Stordalen are dry features underlain by
149 permafrost, with an ALT usually < 0.7 m in late summer; the Sphagnum sites are also
150 underlain by permafrost, representing intermediate thaw features, with an ALT
151 generally thicker than 1.0 m in late summer, and are wetter than the Palsa with water
152 table levels fluctuating close to the ground surface; the Eriophorum sites have no
153 permafrost and are generally wetter than Sphagnum, with water table levels
154 constantly near or above the ground surface (Bäckstrand et al., 2008, 2010; Olefeldt
155 and Roulet, 2012). They are also differentiated in elevation, with Palsa highest,
156 Sphagnum intermediate, and Eriophorum lowest. Therefore these three land cover
157 types have different permafrost regimes and soil water conditions, which support
158 different vegetation compositions (Bäckstrand et al., 2008, 2010). During the last
159 three decades, there have been pronounced shifts in the extent of these three land
160 cover types, with Palsa being converted into Sphagnum or Eriophorum dominated
161 land cover at the north part of the Stordalen mire and both Palsa and Sphagnum being
162 converted into Eriophorum dominated land cover at the south part of the mire
163 (Christensen et al., 2004; Malmer et al., 2005). These three land cover types can be
164 regarded as representing a gradient of permafrost degradation (e.g., Malmer et al.,
165 2005; Johansson T. et al., 2006; Bäckstrand et al., 2010).

166

167 CO₂ and CH₄ fluxes were measured using automated chambers at Stordalen during
168 2003 to 2009. NEE was measured at three sites (i.e., the Palsa, Sphagnum, and
169 Eriophorum sites) to represent three typical land cover types, and CH₄ emissions were
170 consistently observed at the Sphagnum and Eriophorum sites, where water table
171 levels were above or near the peat surface (Bäckstrand et al., 2008, 2010). The Palsa
172 site is relatively dry and its CH₄ flux is near zero (Bäckstrand et al., 2008). For each
173 plot, an auto-chamber system measured CO₂ and total hydrocarbon (THC) fluxes
174 every three hours and there were eight measurements per day. CH₄ fluxes were
175 manually observed approximately three times per week by taking samples from every
176 chamber and these measurements were used to quantify the proportion of CH₄ in the
177 measured THC (Bäckstrand et al., 2008, 2010). Daily NEE and CH₄ fluxes were
178 calculated as average values of eight measurements. During 2003 to 2009, valid rates
179 of daily NEE were calculated for 85-213 days in a year based on the field
180 measurements. Daily CH₄ fluxes were available for 79-116 days in a year, with an
181 exception in 2006 when the instrument was down (Bäckstrand et al., 2008, 2010). In
182 addition, soil thaw depth (measured to 90 cm) and water table depth (WTD) were
183 measured 3-5 times per week from early May to mid October each year (Bäckstrand
184 et al., 2008). Daily meteorological data, including air temperature, precipitation, solar
185 radiation, wind speed, as well as relative humidity, were recorded at the ANS (Figure
186 1). The technical details regarding the measurements of NEE and CH₄ fluxes, and the
187 relevant auxiliary variables were described by Bäckstrand et al. (2008, 2010).

188

189 **2.2 Modification of DNDC**

190 **2.2.1 Overview of the DNDC model**

191 DNDC is a process-based model developed for quantifying C sequestration as well as
192 the emissions of carbon and nitrogen (N) gases from terrestrial ecosystems (Li et al.,
193 1992a, 1992b, 2000; Stange et al., 2000; Zhang et al., 2002). The model has
194 incorporated a relatively complete suite of biophysical and biogeochemical processes,
195 which enables it to compute the complex transport and transformations of C and N in
196 terrestrial ecosystems under both aerobic and anaerobic conditions.

197

198 DNDC is comprised of six interacting sub-models: soil climate, plant growth,
199 decomposition, nitrification, denitrification, and fermentation. The soil climate, plant
200 growth, and decomposition sub-models convert the primary drivers, such as climate,
201 soil properties, vegetation, and anthropogenic activity, into soil environmental factors,
202 such as soil temperature and moisture, pH, redox potential (Eh), and substrate
203 concentrations. The nitrification, denitrification, and fermentation sub-models
204 simulate C and N transformations that are mediated by soil microbes and controlled
205 by soil environmental factors (Li, 2000; Li et al., 2012). In DNDC, NEE is calculated
206 as the difference between net primary production (NPP) and soil microbial
207 heterotrophic respiration (HR). NPP is simulated at daily time step by considering the
208 effects of several environmental factors on plant growth, including radiation, air
209 temperature, soil moisture, and N availability. The model simulates the production of
210 plant litter and incorporates the plant litter into pools of soil organic matter (SOM).
211 HR is calculated by simulating decomposition of SOM. SOM is divided into four
212 pools in DNDC, namely litter, microbes, humads, and passive humus. Each pool is
213 further divided into two or three sub-pools with specific C to N (C/N) ratios and
214 decomposition rates. As a microbially-mediated process, decomposition of each SOM
215 fraction depends on its specific decomposition rate as well as soil thermal and

216 moisture conditions (Li et al., 2012). Methane flux is predicted by modeling CH₄
217 production, oxidation, and transport processes. CH₄ production is simulated by
218 calculating substrate concentrations (i.e., electron donors and acceptors) resulting
219 from decomposition of SOC as well as plant root activities including exudation and
220 respiration, and then by tracking a series of reductive reactions between electron
221 donors (i.e., H₂ and dissolved organic carbon) and acceptors (i.e., NO₃⁻, Mn⁴⁺, Fe³⁺,
222 SO₄²⁻, and CO₂). In DNDC, CH₄ production and oxidation can occur simultaneously
223 within a soil layer but within relatively aerobic and anaerobic micro-sites, whose
224 volumetric fractions are defined by an Eh calculator, a so-called “anaerobic balloon”,
225 embedded in the model framework (Li, 2007). Redox potential, temperature, pH,
226 along with the concentrations of electron donors and acceptors are the major factors
227 controlling the rates of CH₄ production and oxidation. CH₄ is transported from soil
228 into atmosphere via plant-mediated transport, ebullition, and diffusion (Fumoto et al.,
229 2008; Zhang et al., 2002).

230

231 **2.2.2 Soil freeze/thaw and permafrost dynamics**

232 Traditionally, DNDC simulated soil thermal dynamics by a relatively simple module
233 without detailed processes describing the soil thermal regime in the presence of
234 permafrost. It did not explicitly simulate energy exchange within
235 soil-vegetation-atmosphere system, snowpack thermal dynamics, the presence of
236 permafrost, or active layer dynamics (Zhang et al., 2002). However, these processes
237 or environmental factors are important for characterizing the permafrost regime, soil
238 thermal dynamics, soil hydrology, or C and N cycles in high latitudes (e.g.,
239 Riseborough et al., 2008; Waelbroeck, 1993). In order to make DNDC more suitable
240 for northern ecosystems, especially frozen soil conditions, we incorporated a

241 permafrost model, NEST, into the model framework (Zhang et al., 2012). NEST is a
242 process-based model which simulates ground thermal dynamics, soil freeze/thaw
243 dynamics, and permafrost conditions (Zhang et al., 2003). In NEST, soil temperature
244 and permafrost thermal regime are calculated by solving the heat conduction equation,
245 with the upper boundary condition determined by surface energy balance and the
246 lower boundary condition being defined as the geothermal heat flux. The effects of
247 climate, vegetation, snow pack, ground features, and hydrological conditions on the
248 soil thermal regime are incorporated into the model on the basis of energy and water
249 exchanges within soil-vegetation-atmosphere system (Zhang et al., 2003, 2005). To
250 ensure that DNDC simulates permafrost environmental factors and biogeochemistry
251 in synchrony, NEST's functions, which describe soil thermal and hydrologic regimes,
252 were embedded into the framework of DNDC at the model code level. After coupling
253 to NEST, DNDC was able to simulate both the seasonal dynamics of active layer and
254 the long-term variations of permafrost as well as their impacts on biogeochemical
255 processes (Zhang et al., 2012). Therefore, the model should better serve
256 investigations of impacts of climate change on C fluxes in high-latitude ecosystems.

257

258 **2.3 Model application**

259 We performed DNDC simulations for the three typical Stordalen land cover types
260 (Palsa, Sphagnum, and Eriophorum) from 2002 to 2009. Daily meteorological data
261 (i.e., maximum, mean, and minimum air temperature, precipitation, solar radiation,
262 wind speed, and humidity) from 2002 to 2009 recorded at the ANS were collected to
263 support the simulations. All sites had a surface soil layer of peat (0.5 m) overlying a
264 silt soil layer (Rosswallet al., 1975; Rydeñet al., 1980; Olefeldtet al., 2012). The peat
265 had a bulk density of 0.15 g cm^{-3} , SOC content of $0.5 \text{ kg C kg}^{-1} \text{ SDW}$ (soil dry

266 weight), total porosity of 0.9, field capacity of 0.4 (water-filled pore space), wilting
267 point of 0.15 (water-filled pore space), and pH (H₂O) of 5.0, according to
268 observations from Malmer and Walleń (1996), Rydeń et al. (1980), and Öquist and
269 Svensson (2002). The local bedrock is granite (Rosswallet al., 1975) and a thermal
270 conductivity of 2.9 W m⁻¹ °C⁻¹ was used (Clauser and Huenges, 1995). The
271 geothermal heat flux in the study region was estimated as 0.06 W m⁻² (Majorowiczet
272 al., 2011).

273

274 While the three land cover types share common conditions regarding weather,
275 geology, and soil during the simulations, they differ in soil hydrologic conditions and
276 vegetation characteristics. In order to predict the dynamics of water table at the
277 Sphagnum and Eriophorum sites, DNDC used several parameters to estimate lateral
278 flows, including surface inflow rate, maximum water table depths for surface and
279 ground outflows, as well as surface and ground outflow rates (Zhang et al., 2002). We
280 estimated these parameters by comparing the modeled and observed WTD (Table 1).
281 To reduce the influence of WTD prediction-error on soil thermal and biogeochemical
282 processes, the observed WTDs were used during the simulations if the measurements
283 were available, and the simulated WTDs from this calibrated model were used to
284 interpolate daily values between observations. WTD observations at the Sphagnum
285 and Eriophorum sites were made on about one-third of the days across seven growing
286 seasons from 2003 to 2009. For the Palsa site, we assumed that there is no surface
287 lateral inflow and water will flow away each day when the water table is above the
288 land surface or water infiltrates into frost table, based on local studies (Rydeń et al.,
289 1980). DNDC also requires phenological and physiological parameters to simulate
290 plant growth, including maximum biomass production and its partitioning to shoot

291 and root, vegetation C/N ratio, required thermal degree days for vegetation growth,
 292 plant water requirement, and an index of biological N fixation. These parameters for
 293 the three land cover types were determined either based on literature or as model
 294 defaults (Table 2).

295

296 To initialize the soil climate conditions, the soil thermal and hydrological modules of
 297 DNDC were iteratively run by using the climate data in 2002 until the simulated
 298 annual mean soil temperature was stable. Then the vegetation and soil
 299 biogeochemical modules were activated and the model was run continuously from
 300 2002 to 2009. (Note that soil initial conditions have only a small influence on DNDC
 301 output as compared to other factors, therefore, although we did not turn on the
 302 vegetation and soil biogeochemical modules during the initialization of soil climate
 303 conditions, potential errors in soil initial conditions due to this were small.) We
 304 validated the model by using the measured soil thaw depth, NEE, and CH₄ fluxes;
 305 using the sign convention that positive values represent net CO₂ or CH₄ emissions
 306 into the atmosphere and negative fluxes represent net CO₂ or CH₄ uptake. Two
 307 statistical indexes, the relative root mean squared error (RRMSE, equation 1) and the
 308 coefficient of correlation (R, equation 2), were used to quantify the accordance and
 309 correlation between model predictions and field observations (Moriassi et al., 2007).

$$310 \quad RRMSE = \frac{100}{|\bar{o}|} \sqrt{\frac{\sum_{i=1}^n (p_i - o_i)^2}{n}} \quad (1)$$

$$311 \quad R = \frac{\sum_{i=1}^n (o_i - \bar{o})(p_i - \bar{p})}{\sqrt{\sum_{i=1}^n (o_i - \bar{o})^2 \sum_{i=1}^n (p_i - \bar{p})^2}} \quad (2)$$

312 In both equations, o_i and p_i are the observed and simulated values, respectively; \bar{o}

313 and \bar{p} are their averages; and n is the number of values. In addition, we decomposed
 314 the root mean squared error into systematic and unsystematic components by using
 315 the ordinary least square (OLS) method (Willmott, 1982; Willmott et al., 1985). The
 316 systematic and unsystematic root mean squared errors (RMSE_S and RMSE_U) were
 317 calculated with equations 3 and 4, respectively:

$$318 \quad RMSE_S = \sqrt{\frac{\sum_{i=1}^n (\hat{p}_i - o_i)^2}{n}} \quad (3)$$

$$319 \quad RMSE_U = \sqrt{\frac{\sum_{i=1}^n (p_i - \hat{p}_i)^2}{n}} \quad (4)$$

320 In both equations, \hat{p}_i is an OLS estimate of p_i and is derived from the regression of p_i
 321 on o_i by using the ordinary least square method (Willmott, 1982; Willmott et al.,
 322 1985).

323

324 To quantify the differences of C fluxes for the three land cover types across the
 325 permafrost thaw gradient, we analyzed the simulated annual NEE and CH₄ fluxes
 326 from 2003 to 2009. The CH₄ fluxes from dry Palsa were assumed to be zero
 327 (Bäckstrand et al., 2008). We calculated net emissions of greenhouse gases (GHG)
 328 for the three land cover types as CO₂-equivalents by using a 100-year global
 329 warming potential (GWP) of 25 kg CO₂-equivalents kg⁻¹ CH₄ (IPCC, 2007). In
 330 addition, we estimated the possible impacts of permafrost thaw on C fluxes and GHG
 331 emissions for the Stordalen mire based on the model results and changes in the
 332 fractions of the three land cover types from 1970 to 2000.

333

334 **3 Results and analyses**

335 **3.1 Model validation**

336 **3.1.1 Thaw depth**

337 Figure 2 shows the seasonal dynamics of the observed and simulated thaw depth
338 during 2003 to 2009. As field observations demonstrate, thaw rates varied across the
339 three land cover types. At the Palsa site, the maximum thaw depth usually ranged
340 from 45 to 60 cm during the summer seasons from 2003 to 2009, while the soil was
341 often thawed to greater than 90 cm (i.e., below the maximum depth of observations)
342 by August or September at the Sphagnum site and by June or July at the Eriophorum
343 sites. Therefore, the thaw rates were relatively slow, moderate, and rapid at the Palsa,
344 Sphagnum, and Eriophorum sites, respectively. In comparison with the observations,
345 the DNDC model generally captured the differences of thaw depth across the three
346 land cover types as well as their seasonal dynamics (Figure 2). The simulations
347 showed that the dry Palsa site had an active layer thickness of around 55 cm. The
348 thaw depth reached deeper than 100 cm by the end of July to September at the
349 semi-wet Sphagnum site and by June or July at the wet Eriophorum site.

350

351 The model results demonstrated that rate of summer thaw accelerated along the
352 gradient of soil moisture. At the Palsa site, the modeled maximum thaw depth ranged
353 between 50 to 60 cm during the summer seasons from 2003 to 2009, while the soil
354 was often thawed to greater than 90 cm by August at the Sphagnum site and by June
355 or July at the Eriophorum sites. Because water-filled pores have higher thermal
356 conductivity than air-filled pores, DNDC simulated the low, moderate, and high
357 values of thermal conductivity at the dry Palsa, semi-wet Sphagnum, and wet
358 Eriophorum sites, respectively, which consequently resulted in the slow, moderate,
359 and fast rates of summer thaw at these three sites. This explanation is consistent with

360 the conclusion based on the local field study (Rydén and Kostov, 1980). However, a
361 few discrepancies remained between the modeled and observed results, primarily in
362 the soil thaw dynamics at the Sphagnum site, where DNDC overestimated the thaw
363 rate during the late periods of soil thaw in most years (Figure 2h to n). Nevertheless,
364 the comparisons between the simulations and observations indicated that DNDC can
365 reliably predict differences in the dynamics of soil thaw at the three land cover types
366 at Stordalen, which is crucial for correctly simulating the impacts of permafrost thaw
367 on soil hydrology, plant growth, and biogeochemical processes.

368

369 **3.1.2 NEE**

370 Figure 3a-g illustrates the observed and simulated daily NEE at the Palsa site. The
371 daily observations were highly variable and showed a clear seasonal cycle across
372 2003 to 2009, with net CO₂ uptake increasing in early summer, CO₂ uptake most days
373 during mid-summer and net CO₂ emissions in late summer and autumn. In
374 comparison with the measurements, DNDC generally captured the magnitude and
375 seasonal characteristics of daily NEE, although discrepancies existed. The R values
376 were calculated for each year and ranged from 0.40 to 0.69 (Figure 3a-g), indicating
377 that there were significant correlations between the simulated and observed daily
378 NEE in each year ($P < 0.0001$). Table 3 lists the observations and simulations on the
379 cumulative NEE for the seven growing periods from 2003 to 2009. The observed
380 cumulative NEE ranged from -435 to -241 kg CO₂-C ha⁻¹ and the modeled values
381 ranged from -414 to -265 kg CO₂-C ha⁻¹. The calculated RRMSE values varied
382 between 3% and 25% (mean: 13%) across the seven growing seasons and the
383 discrepancies between the simulations and observations were less than the standard
384 deviations of the observed cumulative NEE in each year (Table 3). These results

385 indicate that DNDC successfully simulated the cumulative NEE during growing
386 seasons.

387

388 At the Sphagnum site, the simulated and observed seasonal variations of daily NEE
389 were similar across 2004 to 2009. Both the simulations and observations showed that
390 net CO₂ uptake increased in early summer, prevailed most days during mid-summer,
391 and decreased to net CO₂ emissions in late summer and autumn (Figure 3i-n). The
392 similar patterns suggest that the DNDC model generally captured the seasonal
393 fluctuations of daily NEE over 2004 to 2009, although discrepancies existed in each
394 year. However, it seems systematic biases appeared in 2003. For example, the field
395 observations showed high net uptake rates of CO₂ during 25 May to 22 June in 2003;
396 while the model predicted lower rates (Figure 3h), primarily because of limitations of
397 low solar radiation, air temperature (the mean was 6.0 °C during 25 May to 22 June),
398 and soil temperature on plant productivity. Nonetheless, the modeled and observed
399 daily NEE were significantly correlated in all years ($P < 0.001$ in 2003 and $P < 0.0001$
400 in other years), and R values ranged from 0.32 to 0.78 (Figure 3h-n). The predicted
401 cumulative NEE ranged from -521 to -203 kg CO₂-C ha⁻¹ over seven growing seasons.
402 The results are consistent with the corresponding observations, which ranged from
403 -525 to -212 kg CO₂-C ha⁻¹ (Table 3), with the discrepancies between the simulations
404 and observations close to or less than the standard deviations of the observed
405 cumulative NEE in each year. The values of RRMSE ranged from 1% to 17% with a
406 mean of 6% over 2003 to 2009 (Table 3).

407

408 At the Eriophorum site, both the simulated and observed daily NEE showed similar
409 seasonal patterns across the studied years, excepting 2004 (Figure 3o-u), with net CO₂

410 uptake increasing in early summer, CO₂ uptake most days during mid-summer and
411 net CO₂ emissions in late summer and autumn. The R values ranged from 0.39 to 0.74,
412 which indicates significant ($P < 0.0001$) correlations between the modeled and
413 measured daily NEE in each year during 2003 to 2009. However, we also note
414 systematic deviation between the simulations and measurements in 2004. In this year,
415 the field observations showed persistent low net uptake rates of CO₂ during late May
416 to the end of June; while the model predicted an increasing trend of net CO₂ uptake
417 (Figure 3p), because of increasing solar radiation, air temperature, soil temperature,
418 and soil thaw depth. At the Eriophorum site, the observed daily uptake rates of CO₂
419 were usually higher than that at the Palsa and Sphagnum sites during summer (Figure
420 3). The DNDC model captured the differences across these three sites and the
421 magnitudes of the simulated NEE were comparable with the corresponding
422 observations. The simulations of growing season cumulative NEE ranged from -1078
423 to -365 kg CO₂-C ha⁻¹ during 2003 to 2009, which were close to the observations
424 (ranged from -1118 to -270 kg CO₂-C ha⁻¹). The RRMSE values ranged from 1% to
425 35% (mean: 15%) over 2003 to 2009 (Table 3). The discrepancies between the
426 simulated and observed cumulative NEE were less than the standard deviations of the
427 observations in each year from 2003 to 2007, which indicates DNDC reliably
428 simulated the growing season cumulative NEE over these years. However, the
429 discrepancies were larger than the standard deviations of the observed cumulative
430 NEE in 2008 and 2009 (-571 vs. -471 ± 76 kg C ha⁻¹ in 2008, and -365 vs. -270 ± 59
431 kg C ha⁻¹ in 2009), suggesting that the model may have overestimated the CO₂ uptake
432 during growing season in these two years.

433

434 **3.1.3 Water table and CH₄ fluxes**

435 As shown in Figure 4a-g, WTDs (with positive values for above-ground and negative
436 values for below-ground) fluctuated between -30 to 0 cm at the Sphagnum site, while
437 were generally near or above the ground surface at the Eriophorum site.

438

439 Figure 4h-n compares the observed and simulated daily CH₄ fluxes at the Sphagnum
440 site. As illustrated by Figure 4h-n, the simulated seasonal patterns of daily CH₄ fluxes
441 were close to the observations during the six studied years from 2003 to 2009
442 (excluding 2006, which had no data), with the highest peak appeared in August or
443 September in both the simulations and field measurements. In addition, DNDC
444 simulated small spikes of CH₄ emission a few days after snowmelt and during
445 post-growing season, which also agreed with the observations (Figure 4l-n). The
446 simulated early CH₄ flux spikes were induced by snowmelt and thaw of surface soil
447 layer, which created water saturation in surface peat and thereby supported CH₄
448 production and emission. The high fluxes predicted during post-growing season
449 occurred during occasional thaw of the surface soil layer during the early freezing
450 stage, which provided pathways of releasing for both newly produced methane and
451 methane accumulated in the soil profile. The R values ranged between 0.63 and 0.89
452 over the six years (Figure 4h-n), which indicates the simulated seasonal variation of
453 daily CH₄ fluxes was significantly correlated with the observed seasonal variation in
454 each year ($P < 0.0001$). The similar patterns and significant correlations between the
455 simulated and observed daily CH₄ fluxes suggest that DNDC generally captured the
456 observed seasonal characteristics of CH₄ fluxes, despite a few remaining
457 inconsistencies. The modeled results indicated that the temporal patterns of CH₄
458 fluxes were primarily controlled by soil temperature and the changes of WTD at the
459 Sphagnum site. Simulated daily CH₄ fluxes were positively correlated with soil

460 temperature ($P < 0.0001$) when WTDs were closer to the peat surface than -10 cm
461 (Figure 5a). Simulated daily CH_4 fluxes were also positively correlated with the
462 WTDs ($P < 0.0001$) if the mean of peat layer (0-50 cm) temperature was higher than
463 $2.0\text{ }^\circ\text{C}$ (Figure 5b). Of the six tested sampling periods, the simulated cumulative CH_4
464 fluxes varied from 12.7 to 35.7 $\text{kg CH}_4\text{-C ha}^{-1}$, comparable with the observations,
465 which varied from 9.7 to 30.6 $\text{kg CH}_4\text{-C ha}^{-1}$ (Table 4). The values of RRMSE ranged
466 from 4% to 35% with a mean of 21% (Table 4). The comparison demonstrates that the
467 discrepancies between the simulated and observed cumulative CH_4 fluxes were close
468 to or less than the standard deviations of the observations in each year.

469

470 At the Eriophorum site, the observed CH_4 fluxes usually started to increase early in
471 the growing season, with high peaks appeared during July to September. Then the
472 CH_4 fluxes decreased during the rest of growing season (Figure 4o-u). The simulated
473 seasonal patterns of daily CH_4 fluxes were comparable with the observations, with a
474 generally increasing trend from the early growing season until mid-summer in each
475 year, when the fluxes reached relatively high levels. Then the simulated CH_4 fluxes
476 started to decrease (Figure 4o-u). The correlations between the modeled and
477 measured daily CH_4 fluxes were statistically significant ($P < 0.0001$) in each year,
478 with R values ranging from 0.47 to 0.89 over the six years. These results suggest that
479 DNDC approximately matched the observed daily CH_4 fluxes over the six studied
480 years from 2003 to 2009 (excluding 2006), although discrepancies existed in each
481 year. However, it seems systematic biases existed in 2008. DNDC underestimated the
482 magnitudes of CH_4 fluxes in 2008 and had a relatively later onset of emissions than
483 observations (Figure 4t). The modeled results demonstrated that the temporal patterns
484 of CH_4 fluxes at the Eriophorum site were mainly related to the changes in soil

485 temperature and the associated variations of plant growth and soil decomposition,
486 because of the inundated conditions at this site, which generated constantly wet
487 anaerobic conditions suitable for CH₄ production. Simulated daily CH₄ fluxes were
488 positively correlated with soil temperature (Figure 5c, $P < 0.0001$), and we did not
489 find any correlation between the simulations of daily CH₄ fluxes and WTD (Figure
490 5d). This conclusion is consistent with the field results (e.g., Bäckstrand et al., 2008;
491 Jackowicz-Korczyński et al., 2010). As illustrated by Figure 4h-u, the observed daily
492 CH₄ fluxes at the Eriophorum site were generally higher than that at the Sphagnum
493 site. DNDC captured the differences between these two sites. Of the six tested
494 sampling periods, the observed cumulative CH₄ fluxes ranged from 57.9 to 121 kg
495 CH₄-C ha⁻¹, while the modeled results varied from 45.5 to 113 kg CH₄-C ha⁻¹. The
496 RRMSE values ranged from 3% to 22% with a mean of 12% across these six periods
497 (Table 4). The discrepancies between the simulations and observations were close to
498 or less than the standard deviations of the observed cumulative CH₄ fluxes over the
499 studied years excepting 2003 and 2008, which indicates a good accordance between
500 the simulations and observations of CH₄ fluxes over these years. However, the
501 discrepancy was larger than the standard deviation of the observed cumulative CH₄
502 fluxes in 2003 and 2008 (76.4 vs. 91.8 ± 10.5 kg C ha⁻¹ in 2003, and 45.3 vs. $57.9 \pm$
503 4.42 kg C ha⁻¹ in 2008), suggesting that the model may have underestimated the
504 cumulative CH₄ fluxes in these two years.

505

506 **3.2 Annual C fluxes and net greenhouse gas emissions**

507 In this section, we review simulated annual (not growing season) NEE and CH₄
508 fluxes at the Palsa, Sphagnum, and Eriophorum sites from 2003 to 2009. The
509 simulated annual total NEE varied from -132 to +56.5 (Palsa; mean: -50.9), -492 to

510 -191 (Sphagnum; mean: -342), and -1021 to -399 (Eriophorum; mean: -793) kg
511 CO₂-C ha⁻¹ yr⁻¹, and inter-annual variability of NEE increased with increasing
512 magnitude (Figure 6a). The predictions of annual total NEE were different across the
513 Palsa, Sphagnum, and Eriophorum sites and primarily resulted from differences in
514 environment conditions, including soil temperature, thaw regime (Figure 2), soil
515 moisture content (Figure 4a-g), and vegetation characteristics (as indicated by the
516 different physiological parameters used for simulating plant growth, Table 2). DNDC
517 predicted the highest uptake rates of CO₂ at the Eriophorum site, primarily due to (1)
518 the highest value of the maximum productivity under optimum growing conditions
519 (Table 2); (2) the fastest soil thaw rate (Figure 2), which was favorable for water and
520 nitrogen uptake; and (3) a permanently high water table (Figure 4a-g) which restricted
521 soil heterotrophic respiration and provided abundant water for plant transpiration. The
522 lowest rates of annual total NEE were simulated at the Palsa site, primarily because of
523 (1) the lowest value of the maximum productivity under optimum growing conditions
524 (Table 2), (2) the slowest soil thaw rate and limited summer thaw depths (Figure 2),
525 and (3) a relatively dry soil which restricted plant transpiration and was
526 comparatively favorable for soil decomposition.

527

528 During 2003 to 2009, the simulations of annual total CH₄ fluxes ranged from 17.9 to
529 42.2 (Sphagnum; mean: 32.8) and 72.2 to 125 (Eriophorum; mean: 104) kg CH₄-C
530 ha⁻¹ yr⁻¹. As with NEE simulations, inter-annual variability of CH₄ fluxes increased
531 with increasing annual means (Figure 6a). The annual total CH₄ fluxes were different
532 across the Sphagnum and Eriophorum sites (Figure 6a). Simulated CH₄ fluxes were
533 higher at the Eriophorum site than the Sphagnum site due to: (1) increased rates of
534 CH₄ production due to higher soil temperature and faster thaw rate, (2) a higher water

535 table that supported CH₄ production while restricting CH₄ oxidation, (3) higher plant
536 growth rates and consequently more substrates (e.g., CO₂ and dissolved organic
537 carbon) used for CH₄ production, and (4) accelerated rates of CH₄ transport due to
538 increased plant vascularity.

539

540 Annual net C fluxes were calculated as the sum of annual total NEE and CH₄ fluxes
541 in this study (i.e., horizontal loss of dissolved organic carbon was not considered).
542 Because the CH₄ component was assumed to be zero at the Palsa site, the simulated
543 annual net C fluxes were equal to annual NEE (range: -132 to 56.5 kg C ha⁻¹, mean:
544 -50.9 kg C ha⁻¹) at this site. Simulations of annual net C fluxes ranged between -462
545 to -163 (mean: -309) and -934 to -488 (mean: -689) kg C ha⁻¹ at the Sphagnum and
546 Eriophorum sites, respectively, during 2003 to 2009. These results illustrated that C
547 uptake rates increased along the permafrost thaw gradient at Stordalen (Figure 6b).
548 Net GHG emissions, expressed as CO₂-equivalents, were calculated by considering
549 more powerful radiative forcing potential of CH₄ than CO₂ (25 times over a 100-year
550 horizon). The simulated annual GHG at the Palsa site varied from -485 to 207 kg
551 CO₂-eq. ha⁻¹ yr⁻¹, with a mean of -186 kg CO₂-eq. ha⁻¹ yr⁻¹ from 2003 to 2009. At the
552 Sphagnum and Eriophorum sites, the annual GHG ranged from -806 to 377 and -849
553 to 1905 kg CO₂-eq. ha⁻¹ yr⁻¹, respectively, and the corresponding means were -162
554 and 562 kg CO₂-eq. ha⁻¹ yr⁻¹, respectively. Therefore, the modeled results
555 demonstrated that for the wetter Eriophorum site, higher CH₄ emissions offset its
556 larger net C sink, and the Palsa site was a larger net sink of CO₂-equivalents than the
557 Eriophorum site (Figure 6b).

558

559 **3.3 Possible changes of C fluxes due to permafrost thaw at Stordalen**

560 Interpretation of aerial images of Stordalen showed that the area of ‘hummock’ (Palsa)
561 cover declined from 9.2 to 8.3 ha, while the area of ‘semiwet’ and ‘wet’ (Sphagnum)
562 cover increased from 6.0 to 6.2 ha, and ‘tall graminoid’ (Eriophorum) cover increased
563 from 1.3 to 2.0 ha from 1970 to 2000 (Malmer et al., 2005; Johansson T. et al., 2006).
564 These changes in vegetation cover indicate a trend toward a wetter ecosystem
565 probably as a direct consequence of permafrost thaw at Stordalen. Given that soil
566 thaw rate accelerated under wet conditions (Figure 2), this trend toward a wetter
567 ecosystem (i.e., from Palsa into Sphagnum or Eriophorum) may further accelerate
568 permafrost degradation. By applying the modeled annual CO₂ and CH₄ fluxes to these
569 changes in vegetation cover areas, we estimated an increase of 578 kg C yr⁻¹ (or 35 kg
570 C ha⁻¹ yr⁻¹ for the study area of 16.5 ha) in CO₂ uptake and an increase of 79 kg C yr⁻¹
571 (or 4.8 kg C ha⁻¹ yr⁻¹) in CH₄ emission from 1970 to 2000 at Stordalen. Using a
572 100-year GWP value for methane, the net impact due to the vegetation change is a net
573 CO₂ equivalent emission of 527 kg CO₂-eq. yr⁻¹; i.e., the warming impact of
574 increased CH₄ emission more than offsets the cooling impact of increased CO₂ uptake
575 at the mire. If these fluxes from vegetation cover areas (1970 vs. 2000) were to persist
576 for one to two centuries, an analysis with a simple model of atmospheric perturbation
577 radiative forcing (Frolking et al. 2006) shows that the different atmospheric lifetimes
578 of CO₂ and CH₄ are such that the CO₂ sink would overcome the CH₄ emissions in
579 terms of instantaneous radiative forcing and the climate impact of this vegetation
580 change would eventually switch to a net cooling after about 120 years. Note that the
581 simulated C fluxes over winter are not well-constrained by field data at this time.

582

583 **4. Discussion**

584 **4.1 Validation of DNDC**

585 In this study, we applied the new version of DNDC to simulate soil freeze/thaw
586 dynamics and C fluxes across three typical land cover types (i.e., Palsa, Sphagnum,
587 and Eriophorum) at Stordalen, Sweden, which are considered to represent a gradient
588 of permafrost thaw (Johansson T. et al., 2006; Bäckstrand et al., 2010). Both field
589 observations and DNDC simulations showed significant differences in C fluxes
590 across these three land cover types and the simulated rates of seasonal cumulative C
591 fluxes were comparable with the corresponding measurements for most cases (Tables
592 3 and 4). These results indicate that the model successfully captured the differences in
593 C fluxes among these land cover types. In addition, the model generally captured the
594 magnitudes and temporal dynamics of soil thaw, NEE, and CH₄ fluxes (Figures 2, 3,
595 and 4). The model validation suggests that the enhanced DNDC potentially can be
596 used to predict impacts of permafrost thaw, but cannot yet independently simulate
597 subsequent changes in soil hydrology and vegetation, which influence C dynamics in
598 northern peatlands. We also note some discrepancies between the modeled results and
599 the field measurements.

600

601 Compared to daily observations of NEE, DNDC overestimated CO₂ uptake rates (i.e.,
602 predicted more negative NEE) on a few days during the growing seasons (Figure 3),
603 which may have resulted from over-prediction of photosynthesis, causing DNDC to
604 predict higher NPP. Because meteorological data at the ANS (10 km northwest of
605 Stordalen) were used to support the simulations and photosynthesis is closely related
606 to climate factors, deviations in predicting daily variability in photosynthesis may be
607 caused by lacking site-specific data. Local observations also demonstrated that
608 meteorological conditions were different between Stordalen and ANS (Olefeldt and
609 Roulet, 2012; Rydén, 1980). These differences inevitably affected model simulations

610 of C fluxes. We further calculated the $RMSE_S$ and $RMSE_U$ for daily NEE (Table 5).
611 The results demonstrate that systematic errors accounted for 11%, 25%, and 23% of
612 the mean-square errors in daily NEE at the Palsa, Sphagnum, and Eriophorum sites,
613 respectively. Therefore the discrepancies between the modeled and measured NEE
614 could be primarily attributed to random components, including absence of
615 site-specific data. However, we also note systematic discrepancies between the
616 modeled and observed NEE at both the Sphagnum and Eriophorum sites. Inconsistent
617 with field data in other years, high net uptake rates of CO_2 occurred at the Sphagnum
618 site during 25 May to 22 June in 2003 (Figure 3h-n), even though solar radiation, air
619 temperature, and soil temperature were low (Figure 1) and soil thaw depth was
620 shallow (Figure 2h), causing DNDC to predict lower uptake rates. At the Eriophorum
621 site, the model predicted an increasing trend of net CO_2 uptake (Figure 3p) from late
622 May to the end of June in 2004 because of the increases in solar radiation, air
623 temperature, and soil thaw depth, while the field observations showed persistent low
624 net CO_2 uptake rates. Further studies are needed to clarify the differences in seasonal
625 characteristics of NEE between 2003 and other years at the Sphagnum site, as well as
626 the inconsistencies between the predictions and observations.

627

628 DNDC approximately matched the observed daily CH_4 fluxes at both the Sphagnum
629 and Eriophorum sites (Figure 4). However, we also note a few inconsistencies
630 between the simulations and observations (e.g., in 2003 at the Sphagnum site and in
631 2008 at the Eriophorum site). Model parameters for soil and vegetation characteristics
632 were derived from a number of studies done at Stordalen since the International
633 Biosphere Program in the early 1970s (Sonesson et al., 1980). Because these
634 parameters have strong influences on soil climate, plant growth, and soil

635 biogeochemistry in DNDC, potential biases in inputs could affect model results,
636 including CH₄ fluxes. The calculations of RMSE_S and RMSE_U (Table 5) also
637 demonstrate that most of the mean-square errors in daily CH₄ fluxes were attributable
638 to random errors, including deviations resulted from biases in model inputs, at both
639 the Sphagnum (76%) and Eriophorum (89%) sites.

640

641 In addition, it should be noted that the modeled C fluxes over winter periods remain
642 uncertain because observations utilized for model validation were primarily available
643 during growing seasons. DNDC simulations demonstrated that C fluxes during
644 non-growing season substantially contributed to annual C fluxes at Stordalen. During
645 2003 to 2009, the means of accumulated CO₂ emissions over non-growing seasons
646 were 342, 32.8, and 101 kg CO₂-C ha⁻¹, respectively, at the Palsa, Sphagnum, and
647 Eriophorum sites. Local field studies also indicated that net CO₂ emissions over
648 winter periods significantly contributed to annual NEE at both dry and wet areas
649 (Bäckstrand et al., 2010; Christensen et al., 2012) and accumulation of net CO₂
650 emissions during winter may have made the dry Palsa site a net annual CO₂ source
651 (Bäckstrand et al., 2010). The simulations of average accumulated CH₄ fluxes over
652 non-growing seasons were 9.8 and 13.8 kg CH₄-C ha⁻¹ at the Sphagnum and
653 Eriophorum sites; representing 30% and 13% of mean annual emissions. At the wet
654 area dominated by tall graminoid vegetation, field measurements demonstrated that
655 CH₄ emissions over winter accounted for approximately 19% of the annually emitted
656 CH₄ (Jackowicz-Korczyński et al., 2010). These results indicate that further tests are
657 necessary to verify the model's predictions of C fluxes during winter periods.

658

659 Although the modeled C fluxes were tested against field measurements with

660 encouraging results, we note that uncertainty may exist in simulating individual
661 processes in C transformations. For example, methane flux is predicted by DNDC as
662 the net result of CH₄ production, oxidation, and transport processes. Validating
663 simulations of CH₄ emission against field measurements did not evaluate the
664 DNDC's simulation of these three processes individually. One approach for
665 testing/constraining simulation of the individual processes is to include stable
666 isotopes and isotope fractionation during the processes of methanogenesis (acetate
667 fermentation and CO₂ reduction), methane oxidation, and methane transport (e.g.,
668 Chanton et al., 2005; Corbett et al., 2013). This is planned for future model
669 development.

670

671 **4.2 Permafrost thaw and C fluxes**

672 Our modeled results provide some indications on how C fluxes will change with
673 ongoing permafrost thaw at Stordalen. If the Palsa evolves into Sphagnum or
674 Eriophorum during permafrost thaw, the mire may be able to sequester more
675 atmospheric C, considering the higher rates of net C uptake shown at the Sphagnum
676 or Eriophorum sites (Figure 6b). However, increases of net C uptake were positively
677 correlated with increases of CH₄ emissions across the thaw gradient at Stordalen
678 (Figure 6), indicating that permafrost thaw will generate a tradeoff of GHG. If the net
679 impact is calculated using the GWP methodology (e.g., Shine et al., 1990), the
680 balance depends on the relative rate of changes in CO₂ uptake and CH₄ emissions and
681 the time horizon chosen for the GWP calculation (e.g., Frohking and Roulet, 2007;
682 Whiting and Chanton, 2001).

683

684 By applying the modeled C fluxes to the areal changes of land cover types at

685 Stordalen, we estimated that the net impact due to the vegetation change is a net CO₂
686 equivalent emission of 527 kg CO₂-eq. yr⁻¹ from 1970 to 2000 at Stordalen. However,
687 it should be noted that this result was calculated by assuming constant annual
688 emissions (equal to the means simulated by DNDC from 2003 to 2009) between 1970
689 and 2000 and the modeled results showed obvious inter-annual variability in both
690 NEE and CH₄ fluxes (Figure 6), and it is not known when during 1970-2000 the
691 land-cover change occurred. If the net impact is calculated by considering the
692 inter-annual variability of C fluxes, the estimation of a net CO₂ equivalent emission
693 from 1970 to 2000 is not significant (P = 0.07) higher than zero. Johansson T. et al.
694 (2006) also used a 100-year GWP value for methane, but treated their ‘wet’ cover
695 somewhat differently – equivalent to ‘semi-wet’ (Sphagnum) for NEE due to
696 similarity in vegetation composition, but with a higher value for CH₄ emission as it
697 was an inundated area. Because the ‘wet’ area was nearly 30% of the study region and
698 expanded from 1970 to 2000, Johansson T. et al. (2006) estimated that the mire was a
699 GHG source in terms of CO₂ equivalents to the atmosphere, and they reported an
700 increase of 47% in net radiative forcing from 1970 to 2000 by considering the fluxes
701 during growing season. Our analysis estimated that the mire was a GHG sink due to a
702 lower value for CH₄ emission in ‘wet’ areas, and yielded an overall decrease of 27%
703 in net radiative cooling from 1970 to 2000. The differences and uncertainties in these
704 interpretations illustrate an important scaling challenge – how many land cover
705 classes are needed and what are the most important distinctions to consider? This can
706 be evaluated in future analyses by comparison of up-scaling flux by aerial fractions of
707 land cover with multi-year eddy covariance tower fluxes. Flux towers are now
708 operating at Stordalen under the European Integrated Carbon Observation System
709 (ICOS) program (Paris et al., 2012).

710

711 **4.3 Modeling impacts of permafrost thaw on C fluxes**

712 Modeling impacts of permafrost thaw on C fluxes is in a very early stage, and much
713 additional work is required for a more complete treatment of all of the processes
714 involved. As shown in this and other studies (e.g., Olefeldt et al., 2013), NEE and
715 CH₄ fluxes are strongly controlled by soil water regime and vegetation characteristics,
716 which stresses the importance of considering changes in soil hydrology and
717 vegetation when predicting responses of C turnover to climate change in permafrost
718 ecosystems. Although changes in wetland cover and vegetation have been observed
719 along with permafrost degradation in northern peatlands (e.g., Goetz et al., 2011;
720 Smith et al., 2005), most modeling work that predicts impacts of climate change on C
721 turnover are based on static distribution of wetlands and vegetation (Bohn and
722 Lettenmaier, 2010). Therefore biases may result from neglecting changes in water
723 table regime and vegetation transitions along with permafrost thaw. In this study, we
724 determined different soil water conditions for the three land cover types at Stordalen
725 by combining the observed WTD and the hydrological module of DNDC. The
726 required hydrological parameters were estimated by calibrating against WTD datasets
727 (Table 1). While these parameters were empirically determined, they are consistent
728 with the general topography of Stordalen, with the Palsa surface elevated 0.5-2.0 m
729 above the Eriophorum surface, and the Sphagnum surface at intermediate elevation
730 (Olefeldt and Roulet, 2012). However, it should be noted that sufficient WTD data
731 are required for calibrating these hydrological parameters if the model is to be applied
732 to other peatlands. Although different WTD and vegetation characteristics were used
733 as inputs for different land cover types to represent changes in soil water regime and
734 vegetation along with permafrost thaw at Stordalen, it would be ideal to incorporate

735 these changes dynamically into the model's framework for better understanding how
736 permafrost thaw affect landscape wetness and how this in turn affect vegetation and C
737 fluxes. Our efforts of incorporating a permafrost model should provide a sound
738 approach for the model to incorporate the processes related to changes in soil water
739 regime and vegetation along with permafrost thaw, although important additional
740 processes needed in a comprehensive biogeochemical model fully functional for
741 northern ecosystems.

742

743 **5. Conclusions**

744 Climate warming and associated permafrost degradation are expected to have
745 significant impacts on the C balance of permafrost ecosystems but the magnitude is
746 uncertain. We incorporated a permafrost model, NEST, into a biogeochemical model,
747 DNDC, to model C dynamics in high-latitude ecosystems. The enhanced DNDC
748 model was applied to assess effects of permafrost thaw on C fluxes of a sub-arctic
749 peatland at Stordalen, Sweden. DNDC simulated soil freeze/thaw dynamics and C
750 fluxes across three typical land cover types (i.e., Palsa, Sphagnum, and Eriophorum)
751 at Stordalen, which span a gradient in the processes of permafrost thaw. Model results
752 were tested against multi-year field measurements. The model validation indicates
753 that DNDC was able to capture differences in seasonal soil thaw, NEE, and CH₄
754 fluxes across the Palsa, Sphagnum, and Eriophorum sites at Stordalen. In addition, the
755 simulated magnitudes and temporal dynamics of soil thaw, NEE, and CH₄ fluxes were
756 in general agreement with field measurements. Consistent with the results from field
757 studies, the modeled C fluxes across the permafrost thaw gradient demonstrate that
758 permafrost thaw and the associated changes in soil hydrology and vegetation increase
759 net uptake of C from atmosphere, but also increase the radiative forcing impacts on

760 climate due to increased CH₄ emission. By using the modeled annual C fluxes and
761 reported areas of vegetation cover in 1970 and 2000, we estimated that the Stordalen
762 mire was a net GHG sink (using a 100-year GWP value for methane) and yielded an
763 overall decrease of 27% in net radiative cooling from 1970 to 2000.

764

765 **Acknowledgements**

766 This study was supported by the NASA Terrestrial Ecology Program
767 (NNX09AQ36G), the US Department of Energy (DE-SC0004632), and the US
768 National Science Foundation (ARC-1021300). We thank the Abisko Scientific
769 Research Station for providing the meteorological data. We thank N. T. Roulet and an
770 anonymous reviewer for comments and suggestions that improved the manuscript.

771

772 **References**

- 773 ACIA: Arctic climate impact assessment: scientific report, Cambridge University
774 Press, New York, 2005.
- 775 Aerts, R., Wallén, B., and Malmer, N.: Growth-limiting nutrients in
776 *Sphagnum*-dominated bogs subject to low and high atmospheric nitrogen supply, *J.*
777 *Ecol.*, 80, 131-140, 1992.
- 778 Aerts, R., Wallén, B., Malmer, N., and de Caluwe, H.: Nutritional constraints on
779 *Sphagnum*-growth and potential decay in northern peatlands, *J. Ecol.*, 89, 292-299,
780 2001.
- 781 Avis, C. A., Weaver, A. J., and Meissner, K. J.: Reduction in areal extent of
782 high-latitude wetlands in response to permafrost thaw, *Nat. Geosci.*, 4, 444-448,
783 2011.
- 784 Åkerman, H. J. and Johansson, M.: Thawing permafrost and thicker active layers in
785 sub-arctic Sweden, *Permafrost Periglac.*, 19, 279-292, 2008.
- 786 Bäckstrand, K., Crill, P. M., Mastepanov, M., Christensen, T. R., and Bastviken, D.:
787 Total hydrocarbon flux dynamics at a subarctic mire in northern Sweden, *J.*
788 *Geophys. Res.*, 113, G03026, doi:10.1029/2008JG000703, 2008.
- 789 Bäckstrand, K., Crill, P. M., Jackowicz-Korczyński, M., Mastepanov, M., Christensen,
790 T. R., and Bastviken, D.: Annual carbon gas budget for a subarctic peatland,
791 Northern Sweden, *Biogeosciences*, 7, 95-108, 2010.
- 792 Bohn, T. J. and Lettenmaier, D. P.: Systematic biases in large-scale estimates of
793 wetland methane emissions arising from water table formulations, *Geophys. Res.*
794 *Let.*, 37, L22401, doi: 10.1029/2010GL045450, 2010.
- 795 Callaghan, T. V., Bergholm, F., Christensen, T. R., Jonasson, C., Kokfelt, U., and
796 Johansson, M.: A new climate era in the sub-Arctic: Accelerating climate changes

797 and multiple impacts, *Geophys. Res. Lett.*, 37, L14705, doi:
798 10.1029/2009GL042064, 2010.

799 Chanton, J. P., Chasar, L., Glaser, P. H., and Siegel, D. I.: Carbon and hydrogen
800 isotopic effects in microbial methane from terrestrial environments, In: *Stable*
801 *isotopes and biosphere-atmosphere interactions: processes and biological controls*,
802 Flanagan, L. B., Ehleringer, J. R., and Pataki, D. E., Elsevier, Amsterdam, 85-105,
803 2005.

804 Christensen, T. R., Johansson, T., Åkerman, H. J., Mastepanov, M., Malmer, N.,
805 Friborg, T., Crill, P., and Svensson, B. H.: Thawing sub-arctic permafrost: effects
806 on vegetation and methane emissions, *Geophys. Res. Lett.*, 31, L04501, doi:
807 10.1029/2003GL018680, 2004.

808 Christensen, T. R., Jackowicz-Korczyński, M., Aurela, M., Crill, P., Heliasz, M.,
809 Mastepanov, M., and Friborg, T.: Monitoring the multi-year carbon balance of a
810 subarctic palsamire with micrometeorological techniques, *Ambio*, 41, 207-217,
811 2012.

812 Clauser, C. and Huenges, E.: Thermal conductivity of rocks and minerals, In: *Rock*
813 *Physics & Phase Relations: A Handbook of Physical Constants*, Ahrens, T. J.,
814 AGU, Washington, D. C., 105-126, 1995.

815 Corbett, J. E., Tfaily, M. M., Burdige, D. J., Cooper, W. T., Glaser, P. H., and Chanton,
816 J. P.: Partitioning pathways of CO₂ production in peatlands with stable carbon
817 isotopes, *Biogeochemistry*, 114, 327-340, doi: 10.1007/s10533-012-9813-1, 2013.

818 Davis, N.: *Permafrost: A Guide to Frozen Ground in Transition*, University of Alaska
819 Press, Fairbanks, AK, 2001.

820 Dorrepaal, E., Toet, S., van Logtestijn, R. S. P., Swart, E., van de Weg, M. J.,
821 Callaghan, T. V., and Aerts, R.: Carbon respiration from subsurface peat

822 accelerated by climate warming in the subarctic, *Nature*, 460, 616-619, 2009.

823 Frohking, S., Roulet, N., and Fuglestedt, J.: How northern peatlands influence the
824 Earth's radiative budget: Sustained methane emission versus sustained carbon
825 sequestration, *J. Geophys. Res.*, 111, G01008, doi:10.1029/2005JG000091, 2006.

826 Frohking, S. and Roulet, N. T.: Holocene radiative forcing impact of northern peatland
827 carbon accumulation and methane emissions, *Glob. Change Biol.*, 13, 1079-1088,
828 2007.

829 Frohking, S., Talbot, J., Jones, M., Treat, C. C., Kauffman, J. B., Tuittila, E. S., and
830 Roulet, N. T.: Peatlands in the Earth's 21st century climate system, *Environ. Rev.*,
831 19, 371-396, 2011.

832 Fumoto, F., Kobayashi, K., Li, C., Yagi, K., and Hasegawa, T.: Revising a
833 process-based biogeochemistry model (DNDC) to simulate methane emission
834 from rice paddy fields under various residue management and fertilizer regimes,
835 *Glob. Change Biol.*, 14, 382-402, 2008.

836 Goetz, S. J., Epstein, H. E., Bhatt, U. S., Jia, G. J., Kaplan, J. O., Lischke, H., Yu, Q.,
837 Bunn, A., Lloyd, A. H., Alcaraz-Segura, D., Beck, P. S. A., Comiso, J. C.,
838 Reynolds, M. K., and Walker, D. A.: Recent changes in arctic vegetation: satellite
839 observations and simulation model predictions, In: *Eurasian arctic land cover and*
840 *land use in a changing climate*, Gutman, G. and Reissell, A., Springer,
841 Netherlands, 9-36, 2011.

842 IPCC: *Climate change 2007: the physical science basis*, In: *Contribution of working*
843 *group I to the fourth assessment report of the Intergovernmental Panel on Climate*
844 *Change: "The Physical Science Basis"*, Solomon, S., Qin, D., Manning, M., Chen,
845 Z., Marquis, M., Averyt, K. B., Tignor, M., and Miller, H. L., Cambridge
846 University Press, Cambridge, 2007.

847 Jackowicz-Korczyński, M., Christensen, T. R., Bäckstrand, K., Crill, P. M., Friborg, T.,
848 Mastepanov, M., and Ström, L.: Annual cycle of methane emission from a
849 subarctic peatland, *J. Geophys. Res.*, 115, G02009, doi:10.1029/2008JG000913,
850 2010.

851 James, M., Lewkowicz, A. G., Smith, S. L., and Miceli, C. M.: Multi-decadal
852 degradation and persistence of permafrost in the Alaska Highway corridor,
853 northwest Canada, *Environ. Res. Lett.*, 8, 045013,
854 doi:10.1088/1748-9326/8/4/045013, 2013.

855 Johansson, M., Christensen, T. R., Åkerman, J. H., and Callaghan, T. V.: What
856 determines the current presence or absence of permafrost in the torneträsk region,
857 a sub-arctic landscape in northern Sweden, *Ambio*, 35, 190-197, 2006.

858 Johansson, T., Malmer, N., Crill, P. M., Friborg, T., Åkerman, J., Mastepanov, M., and
859 Christensen, T. R.: Decadal vegetation changes in a northern peatland, greenhouse
860 gas fluxes and net radiative forcing, *Glob. Change Biol.*, 12, 2,352-2,369, doi:
861 10.1111/j.1365-2486.2006.01267.x, 2006.

862 Kirschke, S., Bousquet, P., Ciais, P., Saunois, M., Canadell, J. G., Dlugokencky, E. J.,
863 Bergamaschi, P., Bergmann, D., Blake, D. R., Bruhwiler, L., Cameron-Smith, P.,
864 Castaldi, S., Chevallier, F., Feng, L., Fraser, A., Heimann, M., Hodson, E. L.,
865 Houweling, S., Josse, B., Fraser, P. J., Krummel, P. B., Lamarque, J., Langenfelds,
866 R. L., Le Quere, C., Naik, V., O'Doherty, S., Palmer, P. I., Pison, I., Plummer, D.,
867 Poulter, B., Prinn, R. G., Rigby, M., Ringeval, B., Santini, M., Schmidt, M.,
868 Shindell, D. T., Simpson, I. J., Spahni, R., Steele, L. P., Strode, S. A., Sudo, K.,
869 Szopa, S., van der Werf, G. R., Voulgarakis, A., van Weele, M., Weiss, R. F.,
870 Williams, J. E., and Zeng, G.: Three decades of global methane sources and sinks,
871 *Nat. Geosci.*, 6, 813-823, doi: 10.1038/NGEO1955, 2013.

872 Kokfelt, U., Reuss, N., Struyf, E., Sonesson, M., Rundgren, M., Skog, G., Rosén, P.,
873 and Hammarlund, D.: Wetland development, permafrost history and nutrient
874 cycling inferred from late Holocene peat and lake sediment records in subarctic
875 Sweden, *J. Paleolimnol.*, 44, 327-342, 2010.

876 Koven, C. D., Ringeval, B., Friedlingstein, P., Ciais, P., Cadule, P., Khvorostyanov, D.,
877 Krinner, G., and Tarnocai, C.: Permafrost carbon-climate feedbacks accelerate
878 global warming, *P. Natl. Acad. Sci. USA*, 108, 14,769-14,774, 2011.

879 Li, C.: Modeling trace gas emissions from agricultural ecosystems, *Nutr. Cycl.*
880 *Agroecos.*, 58, 259-276, doi:10.1023/A:1009859006242, 2000.

881 Li, C.: Quantifying greenhouse gas emissions from soils: scientific basis and modeling
882 approach, *Soil Sci. Plant Nutr.*, 53, 344-352, 2007.

883 Li, C., Frohking, S., and Frohking, T. A.: A model of nitrous oxide evolution from soil
884 driven by rainfall events: 1. Model structure and sensitivity, *J. Geophys. Res.*, 97,
885 9,759-9,776, 1992a.

886 Li, C., Frohking, S., and Frohking, T. A.: A model of nitrous oxide evolution from soil
887 driven by rainfall events: 2. Model applications, *J. Geophys. Res.*, 97, 9,777-9,783,
888 1992b.

889 Li, C., Aber, J., Stange, F., Butterbach-Bahl, K., and Papen, H.: A process-oriented
890 model of N₂O and NO emissions from forest soils: 1. Model development, *J.*
891 *Geophys. Res.*, 105, 4,365-4,384, 2000.

892 Li, C., Salas, W., Zhang, R., Krauter, C., Rotz, A., and Mitloehner, F.: Manure-DNDC:
893 a biogeochemical process model for quantifying greenhouse gas and ammonia
894 emissions from livestock manure systems, *Nutr. Cycl. Agroecos.*, 93, 163-200, doi:
895 10.1007/s10705-012-9507-z, 2012.

896 Lund, M., Lafleur, P. M., Roulet, N. T., Lindroth, A., Christensen, T. R., Aurela, M.,

897 Chojnicki, B. H., Flanagan, L. B., Humphreys, E. R., Laurila, T., Oechel, W. C.,
898 Olejnik, J., Rinne, J., Schubert, P., and Nilsson, M. B.: Variability in exchange of
899 CO₂ across 12 northern peatland and tundra sites, *Glob. Change Biol.*, 16,
900 2,436-2,448, 2010.

901 Majorowicz, J. and Wybraniec, S.: New terrestrial heat flow map of Europe after
902 regional paleoclimatic correction application, *Int. J. Earth Sci.*, 100, 881-887,
903 2011.

904 Malmer, N. and Wallén, B.: Peat formation and mass balance in subarctic
905 ombrotrophic peatlands around Abisko, northern Scandinavia, *Ecol. Bull.*, 45,
906 79-92, 1996.

907 Malmer, N., Johansson, T., Olsrud, M., and Christensen, T. R.: Vegetation, climatic
908 changes and net carbon sequestration in a North-Scandinavian subarctic mire over
909 30 years, *Glob. Change Biol.*, 11, 1895-1909, 2005.

910 McGuire, A. D., Anderson, L. G., Christensen, T. R., Dallimore, S., Guo, L., Hayes, D.
911 J., Helmann, M., Lorensen, T. D., Macdonald, R. W., and Roulet, N.: Sensitivity
912 of the carbon cycle in the Arctic to climate change, *Ecol. Monogr.*, 79, 523-555,
913 2009.

914 Moriasi, D. N., Arnold, J. G., Van Liew, M. W., Bingner, R. L., Harmel, R. D., and
915 Veith, T. L.: Model evaluation guidelines for systematic quantification of accuracy
916 in watershed simulations, *T. ASABE*, 50, 885-900, 2007.

917 Nungesser, M. K.: Modelling microtopography in boreal peatlands: hummocks and
918 hollows, *Ecol. Model.*, 165, 175-207, 2003.

919 Olefeldt, D. and Roulet, N. T.: Effects of permafrost and hydrology on the composition
920 and transport of dissolved organic carbon in a subarctic peatland complex, *J.*
921 *Geophys. Res.*, 117, G01005, doi:10.1029/2011JG001819, 2012.

922 Olefeldt, D., Roulet, N. T., Bergeron, O., Crill, P. M., Bäckstrand, K., and Christensen,
923 T. R.: Net carbon accumulation of a high-latitude permafrost tundra mire similar to
924 permafrost-free peatlands, *Geophys. Res. Lett.*, 39, L03501,
925 doi:10.1029/2011GL050355, 2012.

926 Olefeldt, D., Turetsky, M. R., Crill, P. M., and McGuire, A. D.: Environmental and
927 physical controls on northern terrestrial methane emissions across permafrost
928 zones, *Glob. Change Biol.*, 19, 589-603, 2013.

929 Olsrud, M. and Christensen, T. R.: Carbon partitioning in a wet and a semiwet
930 subarctic mire ecosystem based on in situ ¹⁴C pulse-labelling, *Soil Biol. Biochem.*,
931 43, 231-239, 2011.

932 Öquist, M. G. and Svensson, B. H.: Vascular plants as regulators of methane emissions
933 from a subarctic mire ecosystem, *J. Geophys. Res.*, 107, 4580,
934 doi:10.1029/2001JD001030, 2002.

935 Payette, S., Delwaide, A., Caccianiga, M., and Beauchemin, M.: Accelerated thawing
936 of subarctic peatland permafrost over the last 50 years, *Geophys. Res. Lett.*, 31,
937 L18208, doi: 10.1029/2004GL020358, 2004.

938 Paris, J. D., Ciais, P., Rivier, L., Chevallier, F., Dolman, H., Flaud, J. M., Garrec, C.,
939 Gerbig, C., Grace, J., Huertas, E., Johannessen, T., Jordan, A., Levin, I., Papale, D.,
940 Valentini, R., Watson, A., Vesala, T., and ICOS-PP consortium: Integrated Carbon
941 Observation System, *Geophysical Research Abstracts*, 14, EGU2012-12397, 2012.

942 Quinton, W., Hayashi, M., and Chasmer, L.: Permafrost-thaw-induced land-cover
943 change in the Canadian subarctic: implications for water resources, *Hydrol.*
944 *Process.*, 25, 152-158, 2011.

945 Riseborough, D., Shiklomanov, N., Eitzelmueller, B., Gruber, S., and Marchenko, S.:
946 Recent Advances in Permafrost Modelling, *Permafrost Periglac.*, 19, 137-156,

947 2008.

948 Rosswall, T., Flower-Ellis, J. G. K., Johansson, L. G., Jonsson, S., Rydén, B. E., and
949 Sonesson, M.: Stordalen (Abisko), Sweden, *Ecol. Bull.*, 20, 265-294, 1975.

950 Rydén, B. E.: Climatic representativeness of a project period: epilogue of a tundra
951 study, *Ecol. Bull.*, 30, 55-62, 1980.

952 Rydén, B. E. and Kostov, L.: Thawing and freezing in tundra soils, *Ecol. Bull.*, 30,
953 251-281, 1980.

954 Rydén, B. E., Fors, L., and Kostov, L.: Physical properties of the tundra soil-water
955 system at Stordalen, Abisko, *Ecol. Bull.*, 30, 27-54, 1980.

956 Sachs, T., Giebels, M., Boike, J., and Kutzbach, L.: Environmental controls of CH₄
957 emission from polygonal tundra on the micro-site scale, Lena River Delta, Siberia,
958 *Glob. Change Biol.*, 16, 3,096-3,110, 2010.

959 Schneider von Diemling, T., Meinshausen, M., Levermann, A., Huber, V., Frieler, K.,
960 Lawrence, D. M., and Brovkin, V.: Estimating the near-surface permafrost-carbon
961 feedback on global warming, *Biogeosciences*, 9, 649-665, 2012.

962 Schuur, E. A. G., Bockheim, J., Canadell, J. G., Euskirchen, E., Field, C. B.,
963 Goryachkin, S. V., Hagemann, S., Kuhry, P., Lafleur, P. M., Lee, H., Mazhitova, G.,
964 Nelson, F. E., Rinke, A., Romanovsky, V. E., Shiklomanov, N., Tarnocai, C.,
965 Venevsky, S., Vogel, J. G., and Zimov, S. A.: Vulnerability of permafrost carbon to
966 climate change: implications for the global carbon cycle, *BioScience*, 58, 701-714,
967 2008.

968 Schuur, E. A. G., Vogel, J. G., Grummer, K. G., Lee, H., Sickman, J. O., and
969 Osterkamp, T. E.: The effect of permafrost thaw on old carbon release and net
970 carbon exchange from tundra, *Nature*, 459, 556-559, 2009.

971 Schuur, E. A. G., Benjamin, A., and Permafrost Carbon Network: High risk of

972 permafrost thaw, *Nature*, 480, 32-33, 2011.

973 Shine, K. P., Derwent, R. G., Wuebbles, D. F., and Morcrette, J. J.: Radiative forcing of
974 climate, In: *Climate Change: The IPCC Scientific Assessment*, Houghton, J. T.,
975 Jenkins, G. J., and Ephraums, J. J., Cambridge University Press, Cambridge, UK,
976 41-68, 1990.

977 Smith, L. C., Sheng, Y., McDonald, G. M., and Hinzman, L. D.: Disappearing arctic
978 lakes, *Science*, 308, 1429, doi: 10.1126/science.1108142,2005.

979 Sonneson, M., Jonsson, S., Rosswall, T., and Ryden, B. E.: The Swedish IBP/PT tundra
980 biome project: objectives – planning – site, *Ecol. Bull.*, 30, 7-25, 1980.

981 Stange, F., Butterbach-Bahl, K., Papen, H., Zechmeister-Boltenster, S., Li, C., and
982 Aber, J.: A process-oriented model of N₂O and NO emissions from forest soils: 2.
983 Sensitivity analysis and validation, *J. Geophys. Res.*, 105, 4,385-4,398, 2000.

984 Ström, L. and Christensen, T. R.: Below ground carbon turnover and greenhouse gas
985 exchanges in a sub-arctic wetland, *Soil Biol. Biochem.*, 39, 1,689-1,698, 2007.

986 Tarnocai, C., Canadell, J. G., Schuur, E. A. G., Kuhry, P., Mazhitova, G., and Zimov, S.:
987 Soil organic carbon pools in the northern circumpolar permafrost region, *Global*
988 *Biogeochem. Cy.*, 23, GB2023, doi:10.1029/2008GB003327, 2009.

989 Waelbroeck, C.: Climate-soil processes in the presence of permafrost: a systems
990 modelling approach, *Ecol. Model.*, 69, 185-225, 1993.

991 Wania, R., Ross, I., and Prentice, I. C.: Integrating peatlands and permafrost into a
992 dynamic global vegetation model: 1. Evaluation and sensitivity of physical land
993 surface processes, *Global Biogeochem. Cy.*, 23, GB3014,
994 doi:10.1029/2008GB003412, 2009a.

995 Wania, R., Ross, I., and Prentice, I. C.: Integrating peatlands and permafrost into a
996 dynamic global vegetation model: 2. Evaluation and sensitivity of vegetation and

997 carbon cycle processes, *Global Biogeochem. Cy.*, 23, GB3015,
998 doi:10.1029/2008GB003413, 2009b.

999 Whiting, G. J. and Chanton, J. P.: Greenhouse carbon balance of wetlands: methane
1000 emission versus carbon sequestration, *Tellus B*, 53, 521-528, 2001.

1001 Williams, P. J. and Smith, M. W.: *The Frozen Earth: Fundamentals of Geocryology*,
1002 Cambridge University Press, Cambridge, UK, 1989.

1003 Willmott, C. J.: Some comments on the evaluation of model performance, *B. AM.*
1004 *Meteorol. Soc.*, 63, 1,309-1,313, 1982.

1005 Willmott, C. J., Ackleson, S. G., Davis, R. E., Feddema, J. J., Klink, K. M., Legates, D.
1006 R., O'Donnell, J., and Rowe, C. M.: Statistics for the evaluation and comparison
1007 of models, *J. Geophys. Res.*, 90, 8,995-9,005, 1985.

1008 Yu, Z., Loisel, J., Brosseau, D. P., Beilman, D. W., and Hunt, S. J.: Global peatland
1009 dynamics since the Last Glacial Maximum, *Geophys. Res. Lett.*, 37, L13402,
1010 doi:10.1029/2010GL043584, 2010.

1011 Zhang, Y., Li, C., Trettin, C. C., Li, H., and Sun, G.: An integrated model of soil,
1012 hydrology and vegetation for carbon dynamics in wetland ecosystems, *Global*
1013 *Biogeochem. Cy.*, 16, 1061, doi: 10.1029/2001GB001838, 2002.

1014 Zhang, Y., Chen, W., and Cihlar, J.: A process-based model for quantifying the impact
1015 of climate change on permafrost thermal regimes, *J. Geophys. Res.*, 108, 4695,
1016 doi:10.1029/2002JD003354, 2003.

1017 Zhang, Y., Chen, W., Smith, S. L., Riseborough, D. W., and Cihlar, J.: Soil temperature
1018 in Canada during the twentieth century: complex responses to atmospheric climate
1019 change, *J. Geophys. Res.*, 110, D03112, doi:10.1029/2004JD004910, 2005.

1020 Zhang, Y., Sachs, T., Li, C., and Boike, J.: Upscaling methane fluxes from closed
1021 chambers to eddy covariance based on a permafrost biogeochemistry integrated

1022 model, *Glob. Change Biol.*, 18, 1,428-1,440, doi:
1023 10.1111/j.1365-2486.2011.02587.x, 2012.

1024 Zhang, Y., Wang, X., Fraser, R., Olthof, I., Chen, W., McLennan, D., Ponomarenko, S.,
1025 and Wu, W.: Modelling and mapping climate change impacts on permafrost at
1026 high spatial resolution for an Arctic region with complex terrain, *The Cryosphere*,
1027 7, 1121-1137, doi:10.5194/tc-7-1121-2013, 2013.

1028 Zhuang, Q., Romanovsk, V. E., and McGuire, A. D.: Incorporation of a permafrost
1029 model into a large-scale ecosystem model: Evaluation of temporal and spatial
1030 scaling issues in simulating soil thermal dynamics, *J. Geophys. Res.*, 106, 33,
1031 649-33, 670, 2001.

1032 Zhuang, Q., Melillo, J. M., Kicklighter, D. W., Prinn, R. G., McGuire, A. D., Steudler,
1033 P. A., Felzer, B. S., and Hu, S.: Methane fluxes between terrestrial ecosystems and
1034 the atmosphere at northern high latitudes during the past century: a retrospective
1035 analysis with a process-based biogeochemistry model, *Global Biogeochem. Cy.*,
1036 18, GB3010, doi:10.1029/2004GB002239, 2004.

1037 Zhuang, Q., Melillo, J. M., Sarofim, M. C., Kicklighter, D. W., McGuire, A. D., Felzer,
1038 B. S., Sokolov, A., Prinn, R. G., Steudler, P. A., and Hu, S.: CO₂ and CH₄
1039 exchanges between land ecosystems and the atmosphere in northern high latitudes
1040 over the 21st century, *Geophys. Res. Lett.*, 33, L17403, doi:
1041 10.1029/2006GL026972, 2006.

1042

1043 **Tables**

1044 **Table 1** The hydrological parameters used for modeling lateral flows^a.

Sites	SIR	SOD (m)	SOR	GOD (m)	GOR
Sphagnum	1.0	0	1.0	0.25	0.01
Eriophorum	2.0	-0.05	0.3	0.05	0.01

1045 ^a SIR, surface inflow rate, the fraction (m m^{-1}) of rainfall (or water from snow melt)
1046 flowing into the site from its surroundings; SOD, surface outflow depth, the water
1047 table (WT) depth (positive for below-ground and negative for above-ground) above
1048 which surface lateral outflow occurs; SOR, surface outflow rate, the fraction (m m^{-1})
1049 of water above the SOD which will be lost as surface outflow per day; GOD, ground
1050 outflow depth, the deepest WT depth above which ground outflow occurs; GOR,
1051 ground outflow rate, the fraction (m m^{-1}) of water above the GOD which will be lost
1052 as ground outflow per day. These hydrological parameters were determined by
1053 calibrating against datasets of water table depth.

1054

1055 **Table 2** The physiological parameters used for simulating plant growth.

Sites	MP ^a	SRF ^b	C/N ^c	TDD ^d	WR ^e	Vascularity	NFI ^f
Palsa	1000	0.35/0.65	90	1500	100	0	1.0
Sphagnum	1200	0.7/0.3	90	1500	100	0	1.1
Eriophorum	2500	0.5/0.5	90	1500	100	1	1.5

1056 ^a MP, the maximum productivity under optimum growing conditions (kg C ha⁻¹). The
1057 values were estimated from Rosswall et al. (1975), Malmer and Walleń (1996), and
1058 Malmer et al. (2005).

1059 ^b SRF, the shoot and root fractions. The values were estimated from Ström and
1060 Christensen (2007), Olsurd and Christensen (2011). Note that the vegetation at the
1061 Sphagnum site is not 100% moss.

1062 ^c C/N, carbon to nitrogen ratio of the plant biomass. The values were estimated from
1063 Aerts et al. (1992, 2001).

1064 ^d TDD, the required accumulated air temperature heat sum above a 0 °C threshold
1065 during the growing season (unit: °C • day) for full vegetation growth.

1066 ^e WR, amount of water required by the plant (g water g⁻¹ dry matter).

1067 ^f NFI, index of biological nitrogen fixation.

1068

1069 **Table 3** Comparison of the modeled (M) and observed (O) net ecosystem exchanges
 1070 (NEE, in kg C ha⁻¹) of CO₂ during growing periods at the Palsa, Sphagnum, and
 1071 Eriophorum sites^a.

Year	Palsa			Sphagnum			Eriophorum		
	O ^b	M	RRMSE ^c	O	M	RRMSE	O	M	RRMSE
2003	-330[264]	-414	25	-394[59]	-326	17	-1118[219]	-1078	4
2004	-241[269]	-265	10	-441[73]	-452	2	-815[449]	-870	7
2005	-338[369]	-347	3	-525[69]	-521	1	-741[450]	-980	32
2006	-386[283]	-319	17	-356[27]	-330	8	-1034[94]	-1019	1
2007	-338[187]	-353	4	-436[114]	-424	3	-930[208]	-980	5
2008	-399[263]	-328	18	-264[79]	-288	9	-471[76]	-571	21
2009	-435[129]	-380	13	-212[75]	-203	4	-270[59]	-365	35

1072 ^a The growing period in this study is defined as the periods during which
 1073 measurements of continuous net CO₂ uptake were available. To calculate the total
 1074 NEE over the growing period in each year, fluxes for the days lacking measurements
 1075 were determined using the arithmetic mean fluxes of the two closest days when
 1076 observations were performed. Daily fluxes from either direct measurements or
 1077 gap-filling were then summed up to calculate the growing period cumulative NEE.

1078 ^b Each figure number within the bracket is the standard deviation of three (Palsa and
 1079 Sphagnum) or two (Eriophorum) replicate auto-chamber plots.

1080 ^c RRMSE, relative root mean squared error, %.

1081

1082 **Table 4** Comparison of the modeled (M) and observed (O) CH₄ fluxes (in kg C ha⁻¹)
 1083 during six study periods at the Sphagnum and Eriophorum sites^a.

Year	Sphagnum			Eriophorum		
	O ^b	M	RRMSE ^c	O	M	RRMSE
2003	17.2[5.2]	12.2	29	91.8[10.5]	76.4	17
2004	30.6[8.0]	24.3	21	121[14.7]	105	13
2005	25.1[4.7]	24.1	4	108[60.6]	101	7
2007	30.4[7.5]	35.7	18	116[22.2]	113	3
2008	9.7[4.2]	13.1	35	57.9[4.42]	45.3	22
2009	23.2[7.5]	27.5	18	111[21.7]	101	9

1084 ^a The study period is the span during which continuous measurements of daily CH₄
 1085 fluxes were available. To calculate the total CH₄ emissions over the sampling period
 1086 in each year, fluxes for the days lacking measurements were determined using the
 1087 arithmetic mean fluxes of the two closest days when observations were performed.
 1088 Daily fluxes from either direct measurements or gap-filling were then summed up to
 1089 calculate the growing period cumulative CH₄ emissions.

1090 ^b Each figure number within the bracket is the standard deviation of three (Sphagnum)
 1091 or two (Eriophorum) replicate auto-chamber plots.

1092 ^c RRMSE, relative root mean squared error, %.

1093

1094 **Table 5** The systematic and unsystematic root mean squared errors (RMSE_S and
 1095 RMSE_U) between the modeled and observed daily net ecosystem exchanges (NEE) of
 1096 CO₂ and CH₄ fluxes at the Palsa, Sphagnum, and Eriophorum sites.

Sites	NEE (mg C m ⁻² day ⁻¹)		CH ₄ fluxes (mg C m ⁻² day ⁻¹)	
	RMSE _S	RMSE _U	RMSE _S	RMSE _U
Palsa	140	405		
Sphagnum	119	206	4.7	8.4
Eriophorum	298	545	16.7	46.6

1097

1098 **Figure captions**

1099 **Figure 1** Daily average air temperature, wind speed, precipitation, and solar radiation
1100 during 2002 to 2009. Data were recorded at the Abisko Scientific Research Station
1101 (ANS).

1102 **Figure 2** Simulated and observed seasonal dynamics of thaw depth at the Palsa (a to
1103 g), Sphagnum (h to n), and Eriophorum (o to u) sites during 2003 to 2009. The entire
1104 soil layer was thawed at the beginning of field observations (in mid June) at the
1105 Eriophorum site in 2007 (panel s).

1106 **Figure 3** Simulated and observed daily net ecosystem exchange (NEE) of CO₂ (mg C
1107 m⁻² day⁻¹) at the Palsa (a to g), Sphagnum (h to n), and Eriophorum (o to u) sites
1108 during 2003 to 2009. The correlations between the simulated and observed daily NEE
1109 were significant for all cases (P < 0.0001, except for panel i, where P < 0.001). The
1110 observed data are the means of three (Palsa and Sphagnum) or two (Eriophorum)
1111 chamber replicates and standard deviations are not shown for reasons of clarity. Note
1112 that the vertical axis scales for NEE are different across the three sites.

1113 **Figure 4** Simulated (lines) and observed (dots) water table dynamics (a to g), daily
1114 CH₄ fluxes (mg C m⁻² day⁻¹) at the Sphagnum (h to n) and Eriophorum (o to u) sites
1115 during 2003 to 2009. The correlations between the simulated and observed daily CH₄
1116 fluxes were significant for all cases (P < 0.0001). The observed CH₄ fluxes are the
1117 means of three (Sphagnum) or two (Eriophorum) chamber replicates and standard
1118 deviations are not shown for reasons of clarity. Because of instrument problems
1119 (Bäckstrand et al., 2008), observed data were not used for model evaluation in 2006.
1120 Note that the water table depths at both the Sphagnum and Eriophorum sites are
1121 shown in the panels (a to g) and the vertical axis scales for CH₄ fluxes are different

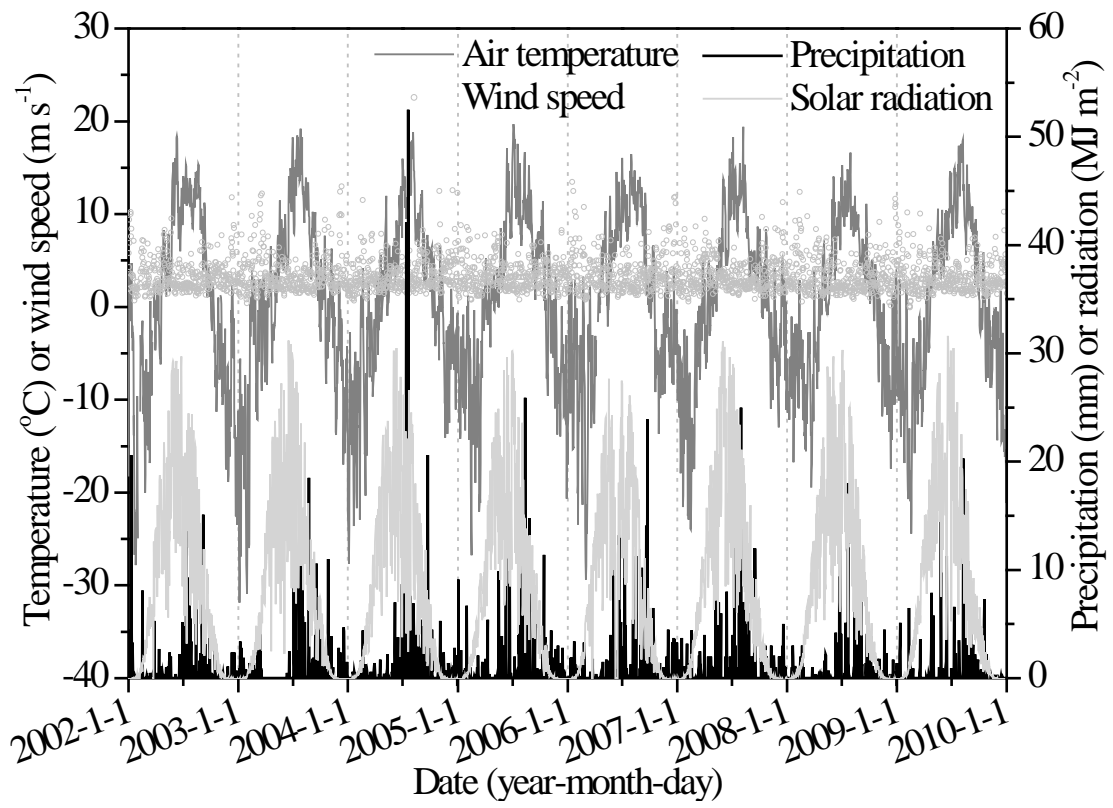
1122 between the two sites.

1123 **Figure 5** Relationships between simulated CH₄ fluxes and average soil (0-50 cm)
1124 temperatures as well as water table depths at the Sphagnum (a and b) and Eriophorum
1125 (c and d) sites. The results shown in the panels (a) and (c) are for periods with water
1126 table depth above -10 cm; the results shown in the panels (b) and (d) are for periods
1127 with average soil temperature (ST, 0-50 cm) > 2 °C. The relationships shown in
1128 panels (a), (b), and (c) were significant (P < 0.0001).

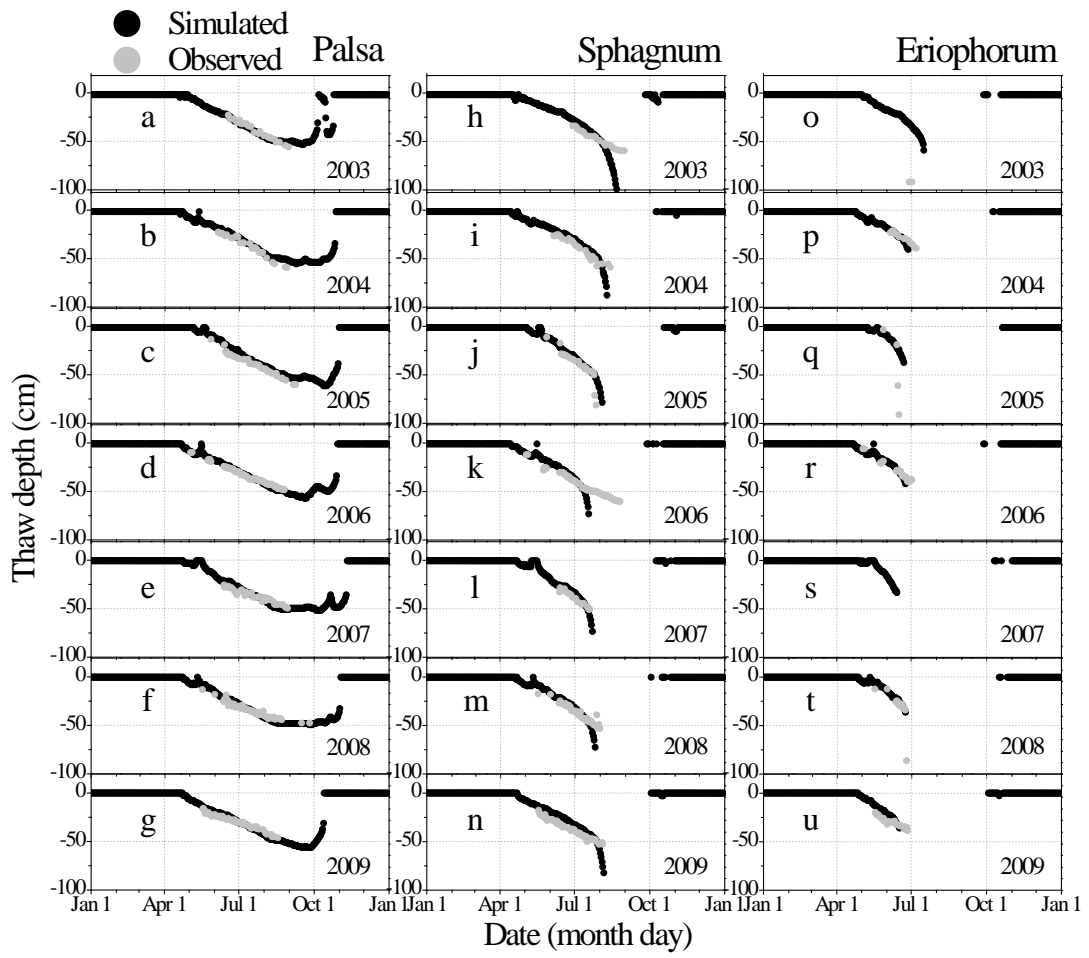
1129 **Figure 6** Simulated net ecosystem exchange (NEE) of CO₂, CH₄ fluxes, net carbon
1130 fluxes, and net emissions of greenhouse gases (GHG) at the Palsa, Sphagnum, and
1131 Eriophorum sites. The CH₄ fluxes from the dry Palsa site were assumed negligible
1132 (here 0), based on field observations. Data are means of annual total fluxes from 2003
1133 to 2009. Vertical bars are standard deviations of annual total fluxes from 2003 to 2009
1134 and indicate inter-annual variations of C gas fluxes.

1135

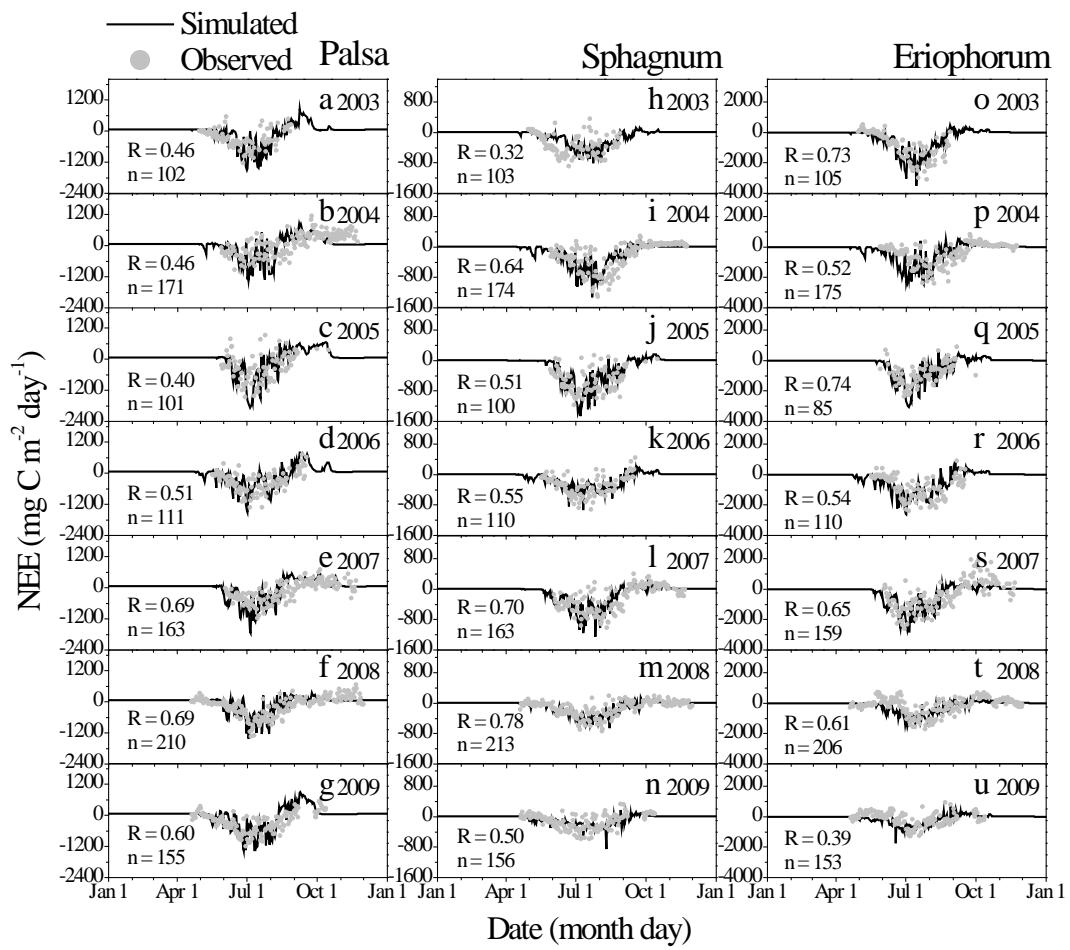
1136 **Figure 1**



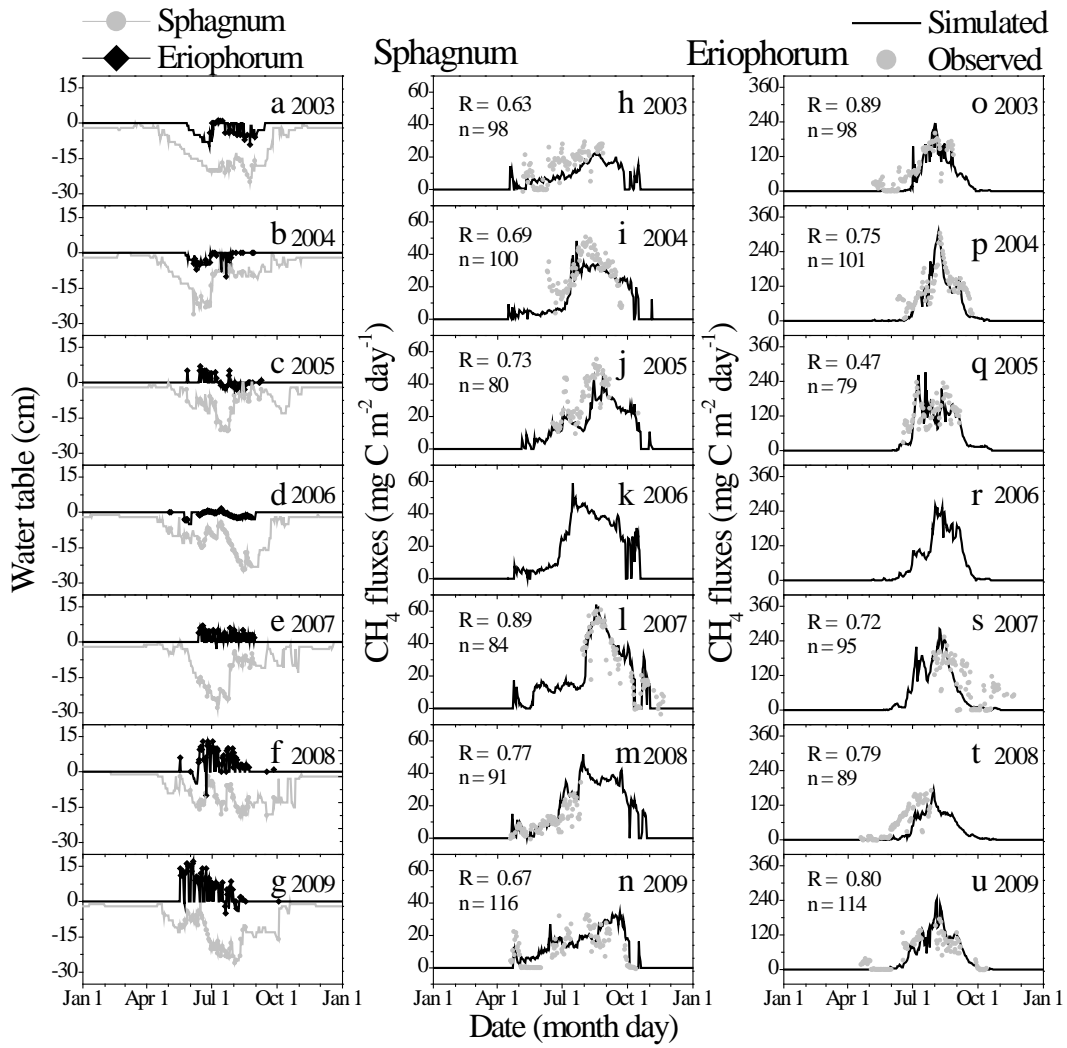
1137
1138



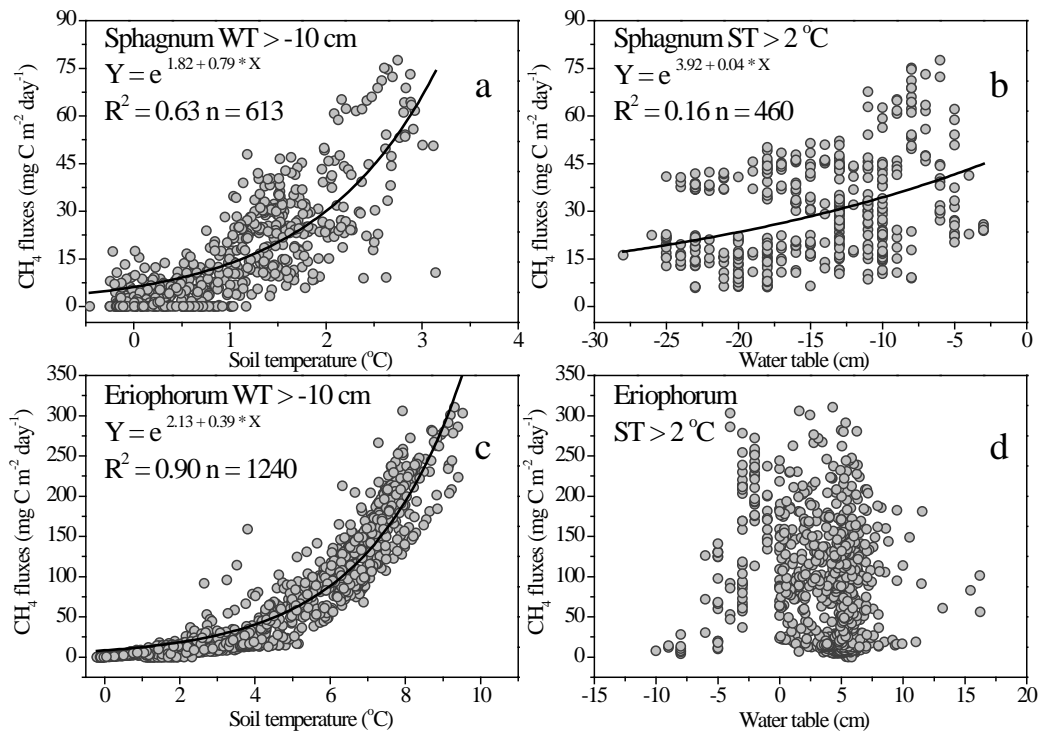
1140
1141



1143
1144



1146
1147



1149
1150

